SEMI-ANNUAL TECHNICAL REPORT NO. 3

NEW TECHNIQUES FOR THE SYNTHESIS OF METALS AND ALLOYS

R. F. Bunshah

THE PROPERTIES OF RARE EARTH METALS AND ALLOYS

D. L. Douglass

UCLA-ENG-7227
April 1972

Security Classification

DOCUMENT CONTROL DATA - R & D

(Security classification of title, body of abstract and indexing annotation must be entered when the overall report is classified)

1. ORIGINATING ACTIVITY (Corporate author)

School of Engineering & Applied Science
University of California at Los Angeles
Los Angeles, California 90024

2a. REPORT SECURITY CLASSIFICATION: Unclassified

2b. GROUP:

3. REPORT TITLE

I. NEW METHODS OF SYNTHESIS OF MATERIALS

II. THE PROPERTIES OF RARE EARTH METALS AND ALLOYS

4. DESCRIPTIVE NOTES (Type of report and inclusive dates)

Semi-Annual Technical Report,

5. AUTHOR(S) (First name, middle initial, last name)

I. R. F. Bunshah

II. D. L. Douglass

6. REPORT DATE	7a. TOTAL NO. OF PAGES	7b. NO. OF REFS
March 1972	59	36

8a. CONTRACT OR GRANT NO.	9a. ORIGINATOR'S REPORT NUMBER(S)
AO #1643	UCLA-ENG-7227
b. PROJECT NO.	
c.	9b. OTHER REPORT NO(S) (Any other numbers that may be assigned this report)
d.	

10. DISTRIBUTION STATEMENT

Distribution of this document is unlimited

11. SUPPLEMENTARY NOTES	12. SPONSORING MILITARY ACTIVITY
	Advanced Research Projects Agency Department of Defense

13. ABSTRACT

Two major areas of effort are encompassed:

I. New Techniques for the Synthesis of Metals and Alloys

The high rate physical vapor deposition (HRPVD) process is to be used for the following:

1. Preparation and characterization of Ni and Ni-20Cr alloy sheet
2. Synthesis of compounds Y_2O_3, TiC, Si_3N_4 by reactive evaporation and their characterization.
3. Dispersion strengthened alloys. Ni-20Cr-Y_2O_3, Ni-20Cr-TiC and Ti-Y_2O_3.

This report describes:

1. The evaporation of a Ni-20Cr alloy from a single rod fed electron beam source.
2. The effect of substrate temperature on the structure and properties of TiC prepared by Activated Reactive Evaporation.

II. The Properties of Rare Earth Metals and Alloys

The oxidation behavior of Ni_3Al and Ni_3Al-0.5Y has been studied at 1200°C in air by thermogravimetric and x-ray analyses. The presence of yttrium has little effect on the oxidation kinetics but markedly reduces spalling of the film during cooling. The effect of preoxidation has also been studied.

DD FORM 1 NOV 65 1473 (PAGE 1)

0102-014-6600

Security Classification

14. KEY WORDS	LINK A		LINK B		LINK C	
	ROLE	WT	ROLE	WT	ROLE	WT
Activated reactive evaporation						
Carbides						
Condensation						
Deposit						
Evaporation						
Evaporation apparatus						
Gadolinium						
High Rate Physical Vapor Deposition Process						
Lanthanum						
Lattice parameter						
Microhardness						
Nichrome						
Nickel						
Nitrides						
Oxidation						
Oxides						
Oxidation mechanism						
Rare-earth additions						
Reactive evaporation						
Refractory carbides						
Scale formation						
Silicon nitride-Si_3N_4						
Substrate						
Synthesis of Materials						
Thickness distribution						
Titanium carbide						
Yttria-Y_2O_3						
Yttrium						

UCLA-ENG-7227
March 1972

SEMI-ANNUAL TECHNICAL REPORT NO. 3

I. New Techniques for the Synthesis of Metals and Alloys
(Principal Investigator - Professor R.F. Bunshah)
Office Phone: (213) 825-2210 or 825-5473

II. The Properties of Rare Earth Metals and Alloys
(Principal Investigator - Professor D.L. Douglass)
Office Phone: (213) 825-1622 or 825-5534

Sponsor: The Advanced Research Projects Agency

Grant No.: DAHC 15-70-G-15

ARPA Order No.: AO 1643

Effective Date: July 1, 1970

Contract Expiration Date: June 30, 1973

Amount of Contract: $298,398

Classification: Un-classified

Materials Department
School of Engineering and Applied Science
University of California
Los Angeles, California

TABLE OF CONTENTS

ABSTRACT

Two major areas of effort are encompassed:

I. New Techniques for the Synthesis of Metals and Alloys

The high rate physical vapor deposition (HRPVD) process is to be used for the following:

1. Preparation and characterization of Ni and Ni-20Cr alloy sheet.
2. Synthesis of compounds Y_2O_3, TiC, Si_3N_4 by reactive evaporation and their characterization.
3. Dispersion strengthened alloys, Ni-20Cr-Y_2O_3, Ni-20Cr-TiC and Ti-Y_2O_3.

This report describes:

(1) The evaporation of a Ni-20Cr alloy from a single rod fed electron beam source.

(2) The effect of substrate temperature on the structure and properties of TiC prepared by Activated Reactive Evaporation.

II. The Properties of Rare Earth Metals and Alloys

The oxidation behavior of Ni_3Al and Ni_3Al-0.5Y has been studied at 1200°C in air by thermograviemetric and x-ray analyses. The presence of yttrium has little effect on the oxidation kinetics but markedly reduces spalling of the film during cooling. The effect of preoxidation has also been studied.

PART I

NEW TECHNIQUES FOR THE SYNTHESIS OF METALS AND ALLOYS (TASKS I, II, AND III)

R. F. Bunshah

INTRODUCTION

This report describes research activities on ARPA Grant No. AO 1643. The scope of the work is divided into two major areas of effort and further subdivided into four tasks as shown be

1. New Techniques for the Synthesis of Metals and Alloys - Tasks I, II, and III. (Professor R.F. Bunshah - Principal Investigator)
2. The Properties of Rare Earth Metals and Alloys - Task IV. (Professor D.L. Douglass - Principal Investigator)

In the following, each of the two topics will be described separately as Part I and Part II of this report with the progress to date.

I. Background

High rate physical vapor deposition (HRPVD) techniques[1-8] are to be used to prepare metallic alloys, ceramics, and metal-ceramic mixtures (dispersion strengthened alloys). The method consists of evaporation of metals, alloys and ceramics contained in water cooled crucibles using high power electron beams. The process is carried out in a high vacuum environment. The use of high power electron beams makes it possible to produce very high evaporation rates. The vapors are collected on heated metallic substrates to produce full density deposits at high deposition rates.

There are three tasks in this section:

Task I: The preparation and characterization of Nickel and Ni-20Cr alloy sheet by the high rate physical vapor deposition process.

Task II: Synthesis and characterization of compounds by Reactive Evaporation. The compounds to be prepared are Y_2O_3, TiC and Si_3N_4.

Task III: Dispersion strengthened alloys produced by HRPVD Process, and their characterization. The specific alloys to be studied are:

A. Ni-20Cr-Y_2O_3 B. Ni-20Cr-TiC C. Ti-Y_2O_3

Single source and two source evaporation methods will be used to produce these alloys.

The HRPVD process has several attractive features:

A. Simple, full density shapes (sheet, foil, tubing) can be produced at high deposition rates, 0.001" per minute thickness increment thus making it an economically viable process.

B. Metals and alloys of high purity can be produced.

C. Very fine grain sizes (1μ grain diameter or smaller) can be produced by controlling substrate temperature. Grain size refinement is

produced by lowering the condensation temperature.

D. An alloy deposit may be produced from a single rod fed source. This occurs because the molten pool at the top of the rod is about 1/4" deep only. The vapor composition is the same as that of the solid rod being fed into the molten pool. At equilibrium, the composition of the molten pool differs from that of the vapor or the solid feed. It is richer in those components having a low vapor pressure. The composition of the vapor is the product of the vapor pressure times the mole fraction of the component. For example, a Ti-6Al-4V alloy deposit where the differences in vapor pressure of Al and V are a factor of 5,000 at 1600°C can be produced by evaporation from a single source. The feed-rod is Ti-6Al-4V and the molten pool is much richer in V than in Al.

E. Two or more sources can be used to simultaneously deposit on the same substrate thus conferring the ability to produce complex alloys. For example, an alloy with a 2 or 3 component solid solution matrix may be evaporated from one source and another metal or ceramic for the dispersed phase from another source. The dispersion size and spacing should be very fine since the deposition is occurring from the vapor phase.

The unique feature of this process is that all of the above benefits can be obtained <u>simultaneously</u>.

It should be noted that the condensation temperature is a very important process variable. Bunshah and Juntz[8] found that for titanium, as the deposition temperature is lowered the grain size of the fully dense deposit becomes finer. At very low temperatures ($\sim$25% of the melting point) the deposit has less than full density.

Since a fine grain sized microstructure represents an optimum condition of strength and toughness in a material, the importance of control over the deposition temperature becomes obvious.

II. Scope of work and progress in reporting period (August 1, 1971 - January 31, 1972)

The main tasks on this contract are the preparation and testing of the various alloys, ceramics and dispersion strengthened alloys as outlined in Section I above. Very essential to the preparation of suitable test specimens are two other factors:

A. Design of the apparatus for high rate physical vapor deposition.

B. Theoretical calculation of the thickness distribution and temperature distribution of the deposited material which is in this case in the form of a sheet.

Both of these tasks are essential preliminaries to the main scope of work. They were completed and described in semi-annual technical report No. 1.[9]

Two papers based on item B above have been published.[10,11]

A. The high rate physical vapor deposition apparatus was reinstalled and put into operation. It is being used for the evaporation of Ni and Ni-20Cr alloys.

B. A theoretical model for the evaporation of an alloy of desired composition from a single rod-feed electron beam source was completed and experimentally verified for the evaporation of the Ni-20Cr alloy. A detailed description is given in Supplement 1 to Part I in this report.

C. The influence of substrate temperature on the structure and properties of TiC deposits produced by Activated Reactive Evaporation was studied.

The microstructure changes from a nodular structure at 500°C to a more dense columnar structure at approximately 800°C and higher. Microhardness measurements show that the high temperature deposits are very hard -- > 4000 kg/mm^2 as measured by Diamond Pyramid and Knoop hardness methods. The low temperature deposits have a microhardness of about 2800-3000 kg/mm^2 which is similar to the values reported in the literature. A detailed progress report is given in Supplement 2 to Part I of this report.

D. Three papers are being submitted for publication in the Journal of Vacuum Science and Technology based on items B and C above and on the Activated Reactive Evaporation Process discussed in Semi-Annual Technical Report No. 2, September 1971[12] on this contract. These papers will also be presented at the Vacuum Metallurgy Conference, American Vacuum Society, June 1972 in Pittsburgh, Pennsylvania.

III. Future Work

In the next half-year period, the following work is scoped.

A. Continuation of the work on deposition of Ni and Ni-20Cr alloy sheets and a study of their structure and properties.

B. Continuation of the work on the synthesis and testing of Y_2O_3, TiC, and Si_3N_4 by reactive evaporation and activated reactive evaporation.

C. Initiation of the work on production of Ni-20Cr alloys containing dispersed phases by HRPVD processes from two evaporation sources.

IV. Personnel

The following personnel have been working on this project in this reporting period.

Principal Investigator - Professor R. F. Bunshah

Graduate Students - Mr. Rao Nimmagadda and Mr. Neil Kane

Technician - Mr. Fred Weiler

REFERENCES

1. Bunshah, R. F., "Superpurification of Metals by Vacuum Distillation: A Theoretical Study," Trans. Vac. Met. Conf., 1963, AVS, 121.

2. Bunshah, R. F., and Juntz, R. S., "Purification of Beryllium by Crucible Free Melting and Distillation Process" in Beryllium Technology, Gordon and Breach, 1964, 1.

3. Bunshah, R. F., "Impurity Removal by Distillation of Beryllium from the Solid State," Proceedings, Int'l. Conf. on Beryllium, Grenoble, France, 1965, Presses Universitaries de France, 108 Blvd. St. Germain, Paris, 6, 63.

4. Bunshah, R. F., and Juntz, R. S., "The Purification of Beryllium by Vacuum Melting followed by Vacuum Distillation in an Electron Beam Furnace with Simultaneous deposition of Sheet," Trans. Vac. Met. Conf., 1966, AVS, 209.

5. Bunshah, R. F., "The Effect of Purification on Some Mechanical Properties of Beryllium," Metals Engineering Quarterly, Nov. 1964, 8.

6. Bunshah, R. F., and Juntz, R. S., "Electron Beam Distillation Furnace for Reactive Metals: Design Considerations and Operating Experience," Trans. Vac. Met. Conf., 1965, AVS, 200.

7. Bunshah, R. F. and Juntz, R. S., "Design Considerations for the Production of Massive Deposits of Alloys by Evaporation from Multiple Electron Beam Heated Sources," Trans. Vac. Met. Conf., 1967, AVS, 799.

8. Bunshah, R. F., and Juntz, R. S., "Influence of Condensation Temperature on Microstructure and Mechanical Properties of Titanium Sheet," to be published.

9. Bunshah, R.F., and Douglass, D. L., Technical Report - UCLA-Eng-7112, March, 1971.

10. Nimmagadda, R., and Bunshah, R.F., J. Vac. Sci. and Tech., December 1971.

11. Chow, R., and Bunshah, R.F. to be published in J. Vac. Sci. and Tech., December 1971.

12. Bunshah, R.F., and Douglass D.L., Technical Report-UCLA-Eng- September 1971.

Supplement 1

PREPARATION OF ALLOY DEPOSITS BY CONTINUOUS ELECTRON BEAM EVAPORATION FROM A SINGLE ROD-FED SOURCE

I. INTRODUCTION

In recent years a great deal of attention has been directed towards the production of self-supported alloy films by high rate physical vapor deposition (HRPVD) processes. The main difficulty with producing an alloy deposit of a desired composition by evaporation is due to different vapor pressures of the components. Several methods have been reported for the deposition of an alloy. They are:

Flash evaporation: In this technique, small amounts of the alloy are dropped on a very hot surface. Total evaporation occurs instantly; thus fractionation of the components is unlikely.

Co-deposition: The technique consists of evaporating alloy constituents from multiple sources at controlled rates so as to deposit an alloy of the desired composition.

Multiple layers: Each of the alloy components is evaporated from a different source to produce alternate layers of predetermined thicknesses depending on the desired alloy composition. Then the deposit is heat treated to homogenize the composition.

Direct evaporation of an alloy from a single source: The evaporation is carried out from a single source of liquid alloy. This is the most desirable of these techniques because vapor distribution for the components is more uniform from a single source than from multiple

sources. Reproducible deposits of required composition have been obtained by this technique.[1] The liquid can be either contained in a wire-fed crucible, as done by Santala and Adams,[2] or can be in the form of a molten pool at the top of a rod, in a rod fed source. Our work is concerned with the latter and the technique is described below.

The schematic experimental arrangement is shown in Fig. 1. Only the top part of the evaporant rod is molten, giving us a progression from solid to liquid to vapor. An alloy constituent evaporates at a rate proportional to the product of its vapor pressure and activity in the pool, which results in the problem that the composition of the vapor is different from that of the liquid. For example, for the deposition of an alloy $A_1 B_1$ in which B has a vapor pressure 10 times that of A, the pool should have a composition $A_{10}B_1$ (assuming ideal solution). This can be circumvented as follows. We start with a rod of composition A_1B_1 so that the initial composition of the molten pool is A_1B_1. B will evaporate faster than A and if we feed rod A_1B_1 continuously into the liquid pool, the pool composition will go from A_1B_1 to $A_{10}B_1$ and remain there. Thus, we have an initial "transient" period where the molten pool composition changes continuously followed by a "steady state" period where it remains constant. This is of considerable practical significance since it eliminates the necessity of fabrication of a sample of the appropriate "steady state" pool composition. One merely lets the rod evaporate until the pool composition reaches the steady state composition, discarding the deposit obtained in this transient period. The duration of transient period and the composition of the deposited alloy during this period are sensitive functions of the rate of evaporation and the volume of the molten pool. In practice it is desirable to have a short "transient period" and to know when the steady state condition is reached.

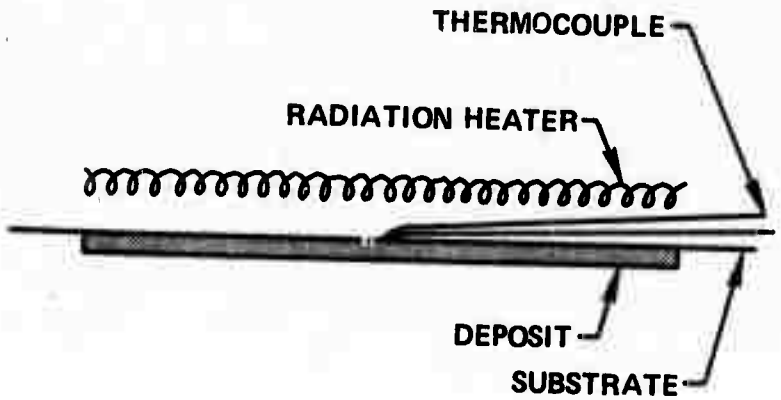

STEADY STATE CONDITIONS:

$p_B^o = 10 p_A^o$

FEED ROD A_1 B_1
MOLTEN POOL A_{10} B_1
VAPOR & DEPOSIT A_1 B_1

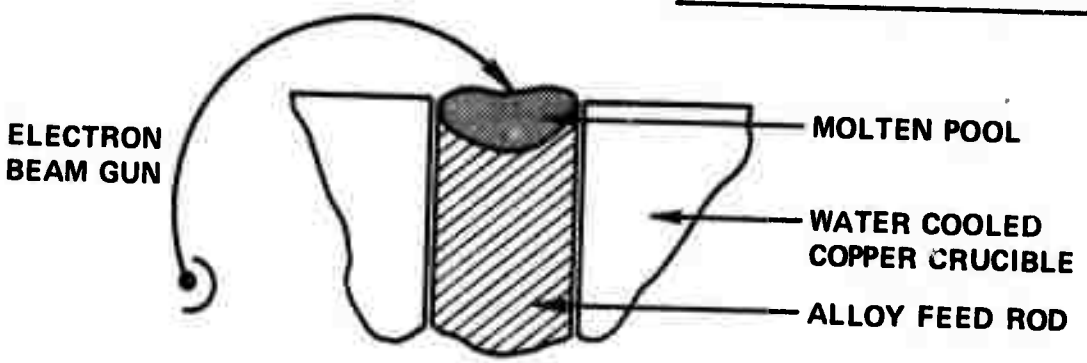

Figure 1. Schematic of Direct Evaporation of an Alloy from a Single Rod-Fed Source.

In this investigation, a model is proposed for the evaporation of alloys from a single rod fed electron beam source. The important predictions of the model are the duration of the transient period and the variations in composition of the alloy deposit with changes in pool temperature and pool volume during evaporation. Experimental work on a Ni-20Cr alloy has been carried out at three different pool temperatures to check the model.

III. MODEL FOR ALLOY EVAPORATION FROM A SINGLE SOURCE

A. Evaporation rate of a constituent in an alloy:

The rate of evaporation of a pure element in vacuum is given by Langmuir[3] based on kinetic theory of gases and the concept of dynamic equilibrium. This relationship has also been applied to alloy evaporation with the assumption, that each species in the solution will evaporate at a rate consistent with its partial pressure over the solution. This assumption has been experimentally verified for Cu-Ag alloys.[2] For a component, i, present in a solution, the Langmuir equation takes the form

$$G_i = \frac{K \alpha_i p_i \gamma_i N_i A}{(M_i T)^{1/2}} \quad \text{moles/sec} \qquad (1)$$

where, G_i = number of moles of component i evaporated per second

α_i = evaporation coefficient of i

p_i = vapor pressure of pure component i at pool temperature T °K in torr

γ_i = activity coefficient of component i in solution

N_i = mole fraction of component i in solution

A = surface area of the pool, cm^2

M_i = molecular weight of component i

T = temperature of the pool, °K

K = constant = 0.0583 (for the above units)

For liquids which evaporate as monomers or as spherically symmetrical molecules the evaporation coefficient will be unity.[4] Generally, metals evaporate as monomers with the exception of elements like antimony which evaporates as Sb_2 molecules.[5] The vapor pressures, activities and activity coefficients can be computed from the published data as discussed below.

B. Vapor pressure of an element:

Vapor pressures of elements are available in several forms, such as tables, charts and empirical equations as a function of temperature. We will use the empirical equation[6]

$$\log p = A\,T^{-1} + B \log T + CT + DT^2 + E \qquad (2)$$

where p = vapor pressure of the element, torr

T = temperature of the element, °K

A, B, C, D and E are constants, characteristic of the element.

C. Activities and activity coefficients of the constituents:

Generally, the activities and activity coefficients for liquid alloys are not available at all temperatures. Assuming regular solution behavior, it is possible to extrapolate γ_i values to other temperatures from the known data at one temperature. Regular solutions are those in which $\overline{F}_i^{xs}$, the excess partial molal free energy is independent of temperature.[7] Mathematically,

$$\overline{F}_i^{xs} = RT \ln \gamma_i \qquad (3)$$

where R = gas constant, cal/mole °K.

From known activity coefficient vs. mol fraction data at one temperature, $\overline{F}_i^{xs}$ is calculated as a function of N_i using equation (3). This data is converted into a fourth order polynomial equation,

$$\bar{F}_i^{xs} = A' N_i^4 + B' N_i^3 + C' N_i^2 + D' N_i + E' \qquad (4)$$

where A', B', C', D' and E' are constants. Using equations (3) and (4), γ_i can be calculated as a function of N_i at any temperature. The results are illustrated in Fig. 2 for Ni-Cr system, using the known activity data[8] at 1600°C as the starting point.

D. Dynamics of Mass Transfer:

The contents of the molten pool can be described by using moles, mass or volume. These quantities are interrelated. However, since the activity coefficients and evaporation rates are direct functions of mole fractions, as expressed in the foregoing calculations, the total number of moles of the alloy constituents in the molten pool is kept constant in our model. Therefore, the number of moles evaporating from the molten pool is equal to the total number of moles fed into the pool, from which the equation of mass balance can be written as,

$$(G_i + G_j + G_k + \ldots) = \pi r^2 \rho S \left(\frac{W_i}{M_i} + \frac{W_j}{M_j} + \frac{W_k}{M_k} + \ldots\right) \qquad (5)$$

where G_i, G_j, G_k, ... = number of moles of each component evaporating from pool per second

W_i, W_j, W_k, ... = weight fractions of components in the feed rod

r = radius of the pool, cm

ρ = density of the alloy, g/cm^3

S = feed rate, cm/sec

Therefore, the feed rate of the rod is given by

$$S = \frac{G_i + G_j + G_k + \ldots}{\pi r^2 \rho \left(\frac{W_i}{M_i} + \frac{W_j}{M_j} + \frac{W_k}{M_k} + \ldots\right)} \qquad (6)$$

E. Composition of the deposit:

The rates of evaporation of each constituent in the pool can be calculated using Langmuir equation as described in an earlier section. Assuming that the composition of the deposit is the same as the composition of the vapor phase, the weight fractions of components in the deposit, W_{Di}, W_{Dj}, W_{Dk}, ..., are given by expressions similar to

$$W_{Di} = \frac{G_i M_i}{G_i M_i + G_j M_j + G_k M_k + \ldots} \qquad (7)$$

F. Composition of the molten pool:

For a pool volume of V cm^3 at T°K, the total number of moles, M, in the liquid pool will be

$$M = V \rho \left(\frac{W_i}{M_i} + \frac{W_j}{M_j} + \frac{W_k}{M_k} + \ldots\right) \qquad (8)$$

The change in the number of moles of the component i, dm_i, in the pool in a short time interval dt is given by

$$dm_i = (\pi r^2 \rho S \frac{W_i}{M_i} - G_i)\, dt \qquad (9)$$

Similarly dm_j, dm_k,... can be computed for the same interval. The number of moles of components i, j, k,... in the pool after a finite time interval Δt is computed by numerical integration of equations of type (9). For the Ni-20Cr alloy, the time interval Δt is chosen such that the composition of Cr in the vapor changes less than 1% by weight in an interval. As evaporation progresses, the fraction of Cr in the pool decreases and that of Ni increases; therefore the activities and activity coefficients change continuously as shown in Fig. 2.

G. Computation of Composition of Pool and Deposit with Time:

The procedure of finding mole fractions, activity coefficients,

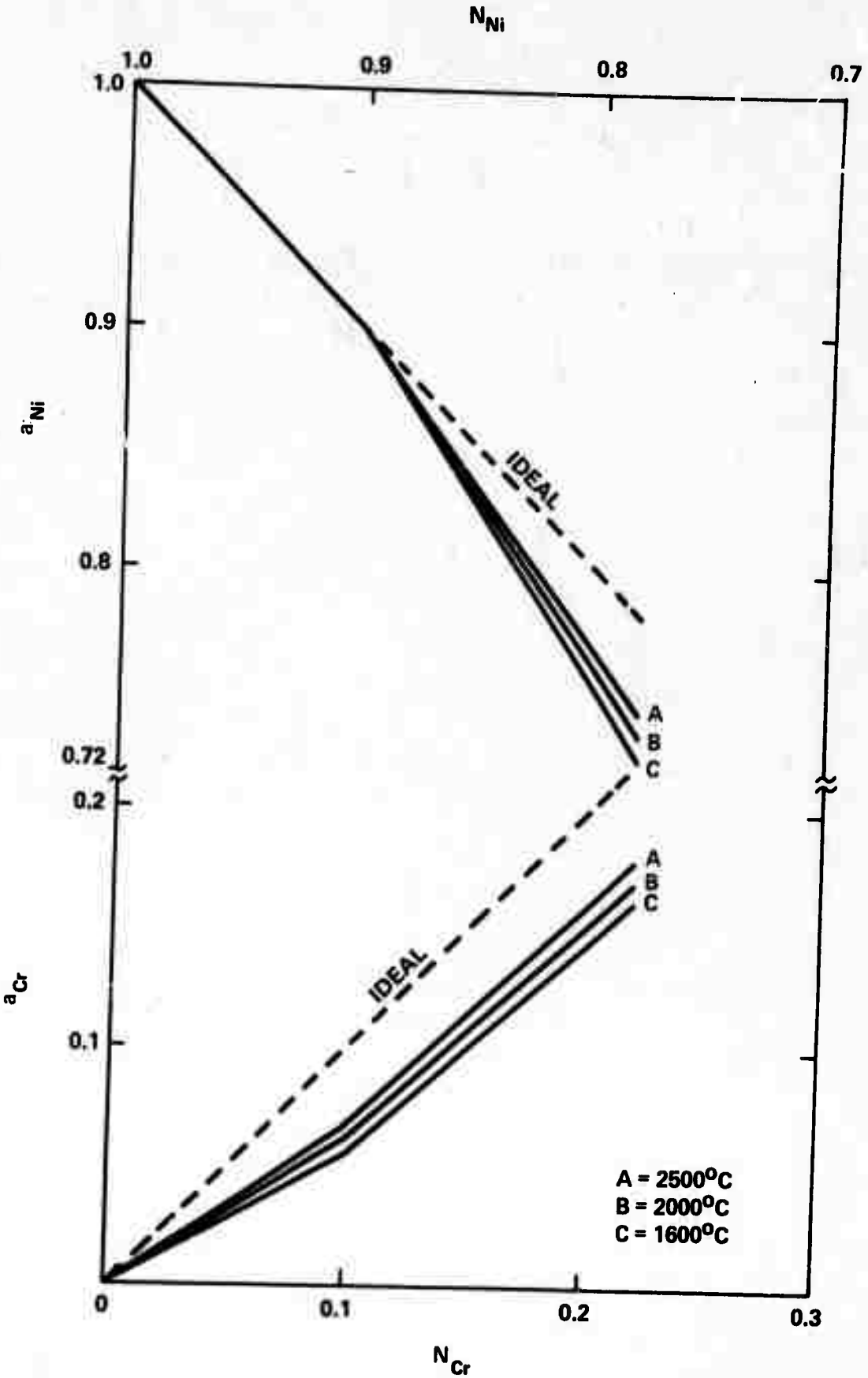

Figure 2. Variation of Activities of Ni and Cr with Mole Fraction at Different Temperatures.

evaporation rates, composition of the deposit, feed rate and number of moles of each constituent in the pool is repeated for each successive time interval, until "steady state" conditions are reached, i.e., the vapor composition becoming the same as the feed rod composition.

IV. EXPERIMENTAL PROCEDURE

High rate physical vapor deposition is carried out in a conventional high vacuum system. The evaporation chamber is a 60 cm diameter 90 cm high water cooled stainless steel bell jar. The evaporation source is a 2.5 cm rod-fed electron beam gun as shown in Fig. 1. The power supply for the gun is an Airco-Temescal (Model CV 30) 30 KW maximum power unit operating at a constant voltage of 10 KV and variable emission current.

The substrate is positioned 15 cm above the molten pool, which is heated from behind by radiation from a 4 KW tungsten resistance heater. The temperature of the substrate is continuously recorded using a chromel-alumel thermocouple. The deposits are collected on a 5 mil stainless steel sheet. The substrates are pre-heated to about 400°C. Higher temperatures were not used, because excessive diffusion may tend to homogenize the deposit along the thickness; and lower temperatures were not used, because the deposits at low temperatures would not be dense. The temperature of the pool is measured by using a two color optical pyrometer. Three different pool temperatures were used, 1665°C, 1800°C and 1875°C; the error in temperature measurement is at least $\pm$ 30°C.[9] All the deposits are made in 10^{-6} torr vacuum or better. The experimental conditions are summarized in table I.

TABLE I

Experimental Conditions of Evaporation of Ni-20Cr Alloy

Evaporation Temperature °C	Temperature of Deposition °C	Rate of Evaporation g/min.	Rate of Deposition $(cm/min) \times 10^{3}$	Volume of Solidified pool (cm^3)
1665	~425	0.42	0.13	1.75
1800	~450	0.82	0.23	2.0
1875	~425	2.00	0.51	2.0

The composition of the Ni-20Cr alloy evaporant rod is given in table II. It is fed upward by a manually-adjusted motor driven mechanism. From the computations shown previously, the feed rate varies during the transient period and should be constant during the steady state period. Since the pool level is judged by eye in the absence of a pool level monitor and the feed mechanism has a limited adjustibility, undershoot and overshoot of the pool level is bound to occur. This is shown as a waviness superimposed on the experimental points. Similar observations were made by Kennedy[10] for the evaporation of iron-chromium and iron-copper alloys.

A small piece of the deposit located near the center is cut and mounted edgewise in bakelite. Special care is taken to ensure that the edges of the deposit are not rounded by sandwitching the deposit between two brass blocks. After polishing, the composition of the deposit is determined by electron microprobe analysis along the thickness of the deposit. The probe samples in steps of 4 μm so that there is a direct correlation between the position of the probe and the time period for that thickness, since the deposition rate is known experimentally.

To determine the volume of the molten pool, approximately 2 cm length of the rod is cut from the top and sliced into half. After polishing, the cross-section is macro-etched using 60 ml water, 35 ml HCl and 5 ml H_2O_2 mixture as etchant. A typical cross-section showing the molten pool is illustrated in Fig. 3. The volume of the molten pool is computed by approximating the shape of the pool into regular geometric shapes.

V. RESULTS AND DISCUSSION

The rates of evaporation, the rates of deposition and the volume of the molten pool are summarized in table I for three experimental temperatures of 1665°C, 1800°C and 1875°C. The rates of evaporation and

Figure 3. Macro-etched cross-section of the evaporated Ni-20Cr rod showing molten pool, heat-affected zone and the feed-rod. Evaporation temperature: 1875°C. Magnification: X 3.5.

TABLE II

Chemical Analysis of Ni-20Cr Alloy

Element	Weight%
Ni	79.44
Cr	19.46
C	0.006
Mn	0.02
Si	0.21
S	0.002
Fe	0.30
Al	0.004
Co	0.12
Cu	0.03
Zr	0.02
Ca	0.03
Pb	0.002

deposition increase with temperature due to the increase in vapor pressures of Cr and Ni and the higher activity coefficients of both Cr and Ni. The volume of the pool did not increase significantly from 1665°C to 1875°C due to greater heat loss by radiation and conduction at higher tempertures.

A. Duration of transient period:

Figures 4, 5 and 6 are plots of % Cr in deposit vs. time for various pool volumes at 1665, 1800 and 1875°C respectively. Figures 7 and 8 are plots of % Cr in deposit vs. time at various pool temperatures for pool volumes of 1.75 and 2 cc. It is observed that the duration of the "transient period" is reduced for higher pool temperatures at constant pool volumes. Similarly, at constant pool temperature, the transient period is shorter with decreasing pool volume.

In Figures 4 to 8, the curve joining the experimental points exhibits a waviness which is due to the manual adjustment of the pool level. This corresponds to a fluctuation of $\pm$ 1% Cr approximately around the average composition. Further it may be noted that the computed curves for the composition of the deposit approach the "steady state" composition, i.e., 20% Cr exponentially. If the end of the "transient period" is defined as the intersection of the computed curve at constant volume with the steady state composition, even a small scatter band around the average "steady state" composition will produce a large variation in the exact time for the end of the computed "transient period." For example, in Fig. 5, for a pool volume of 2 cc, the computed duration of the transient period varies from 18 to 30 minutes when the composition of the deposit decreases from 21 to 20% Cr. Table III shows the comparison between computed and experimental values for the duration of the transient period. The agreement is very good within the precision of the data and therefore

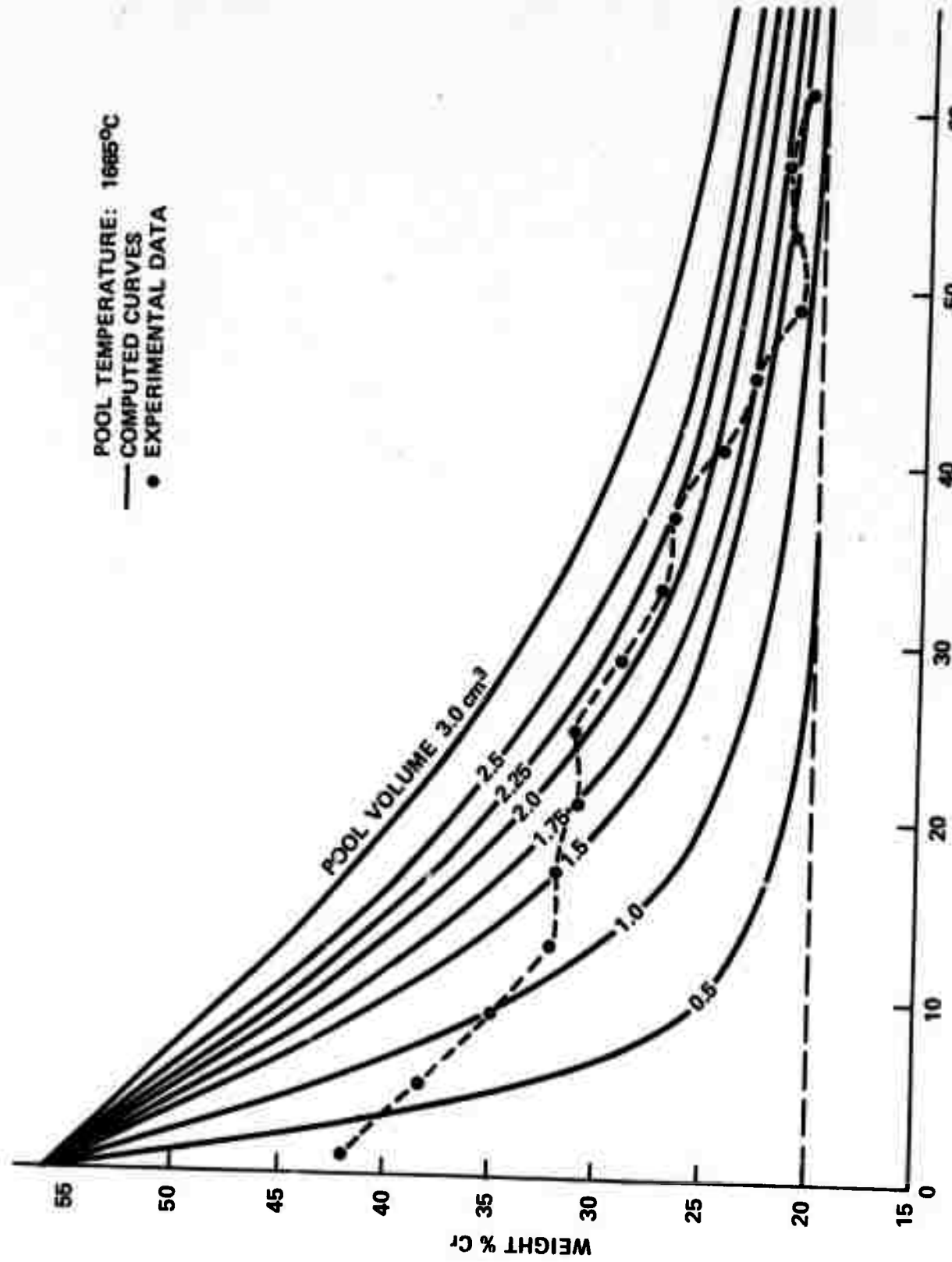

Figure 4. Change in Chromium Content of the Deposit with Time, at Various Pool Volumes at 1685°C.

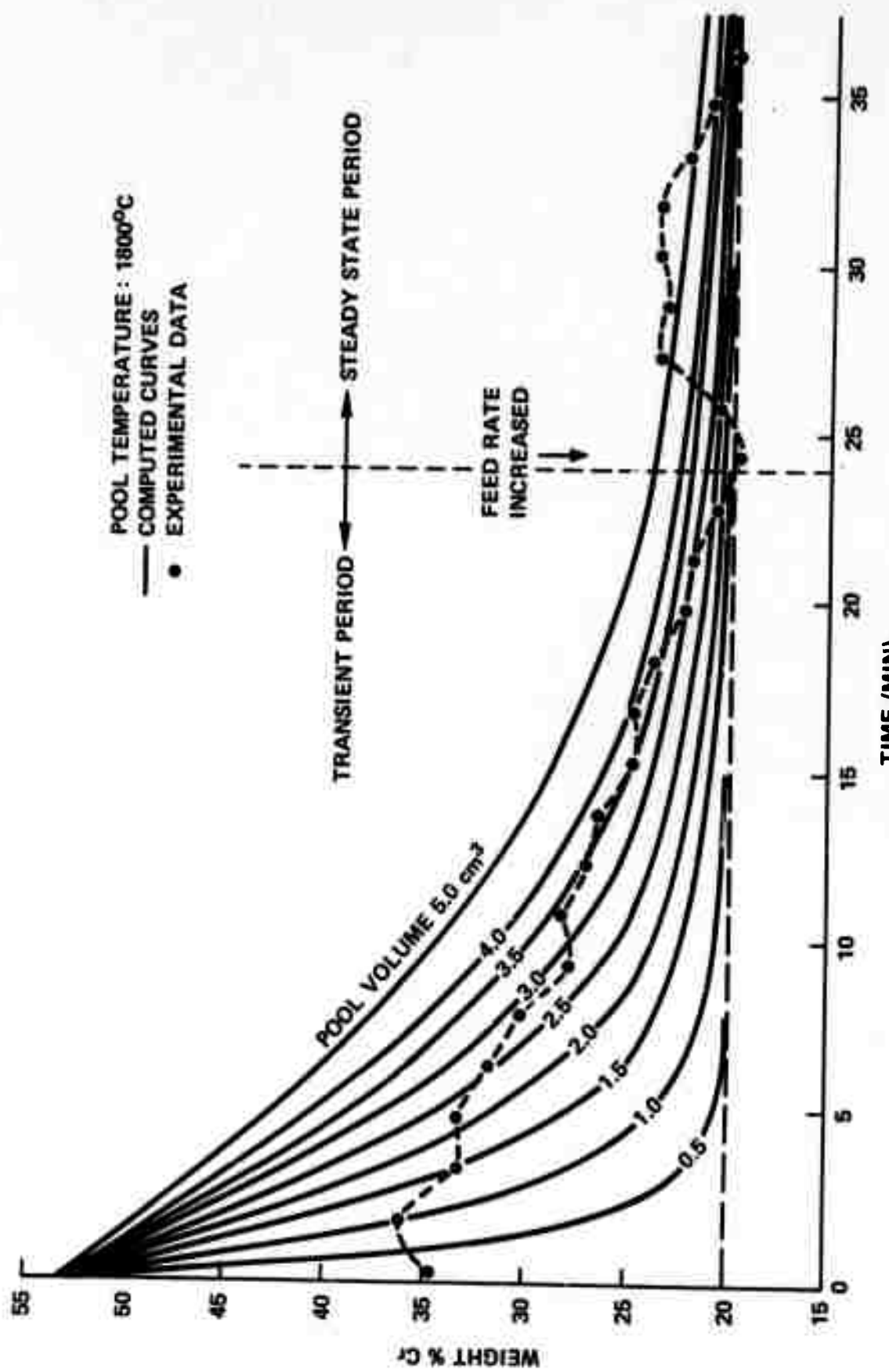

Figure 5. Change in Chromium Content of the Deposit with Time, at Various Pool Volumes at 1800°C.

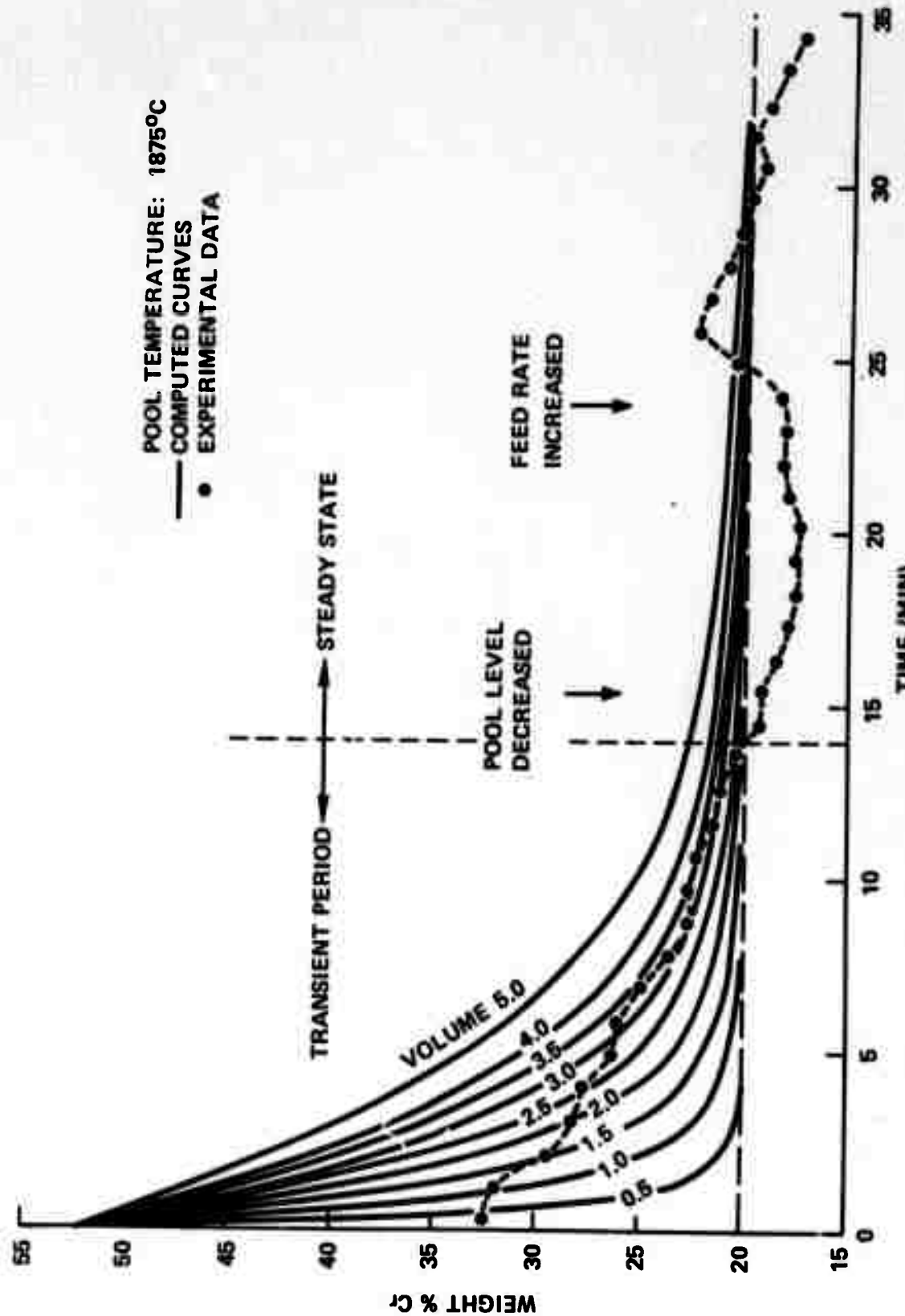

Figure 6. Change in Chromium Content of the Deposit with Time, at Various Pool Volumes at 1875°C.

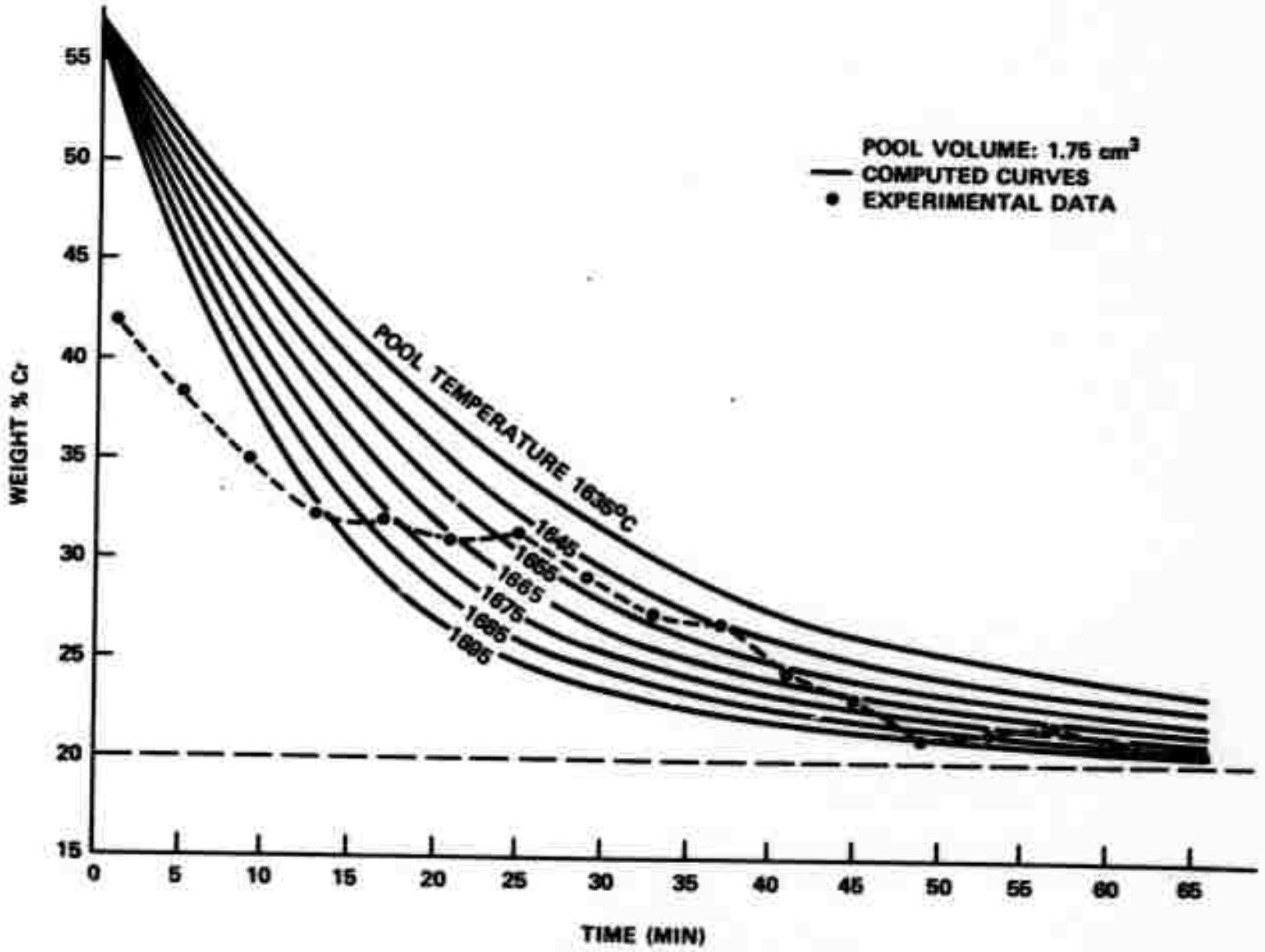

Figure 7. Change in Chromium Content of the Deposit with Time, for Different Pool Temperatures and Constant Pool Volume, 1.75 cm^3.

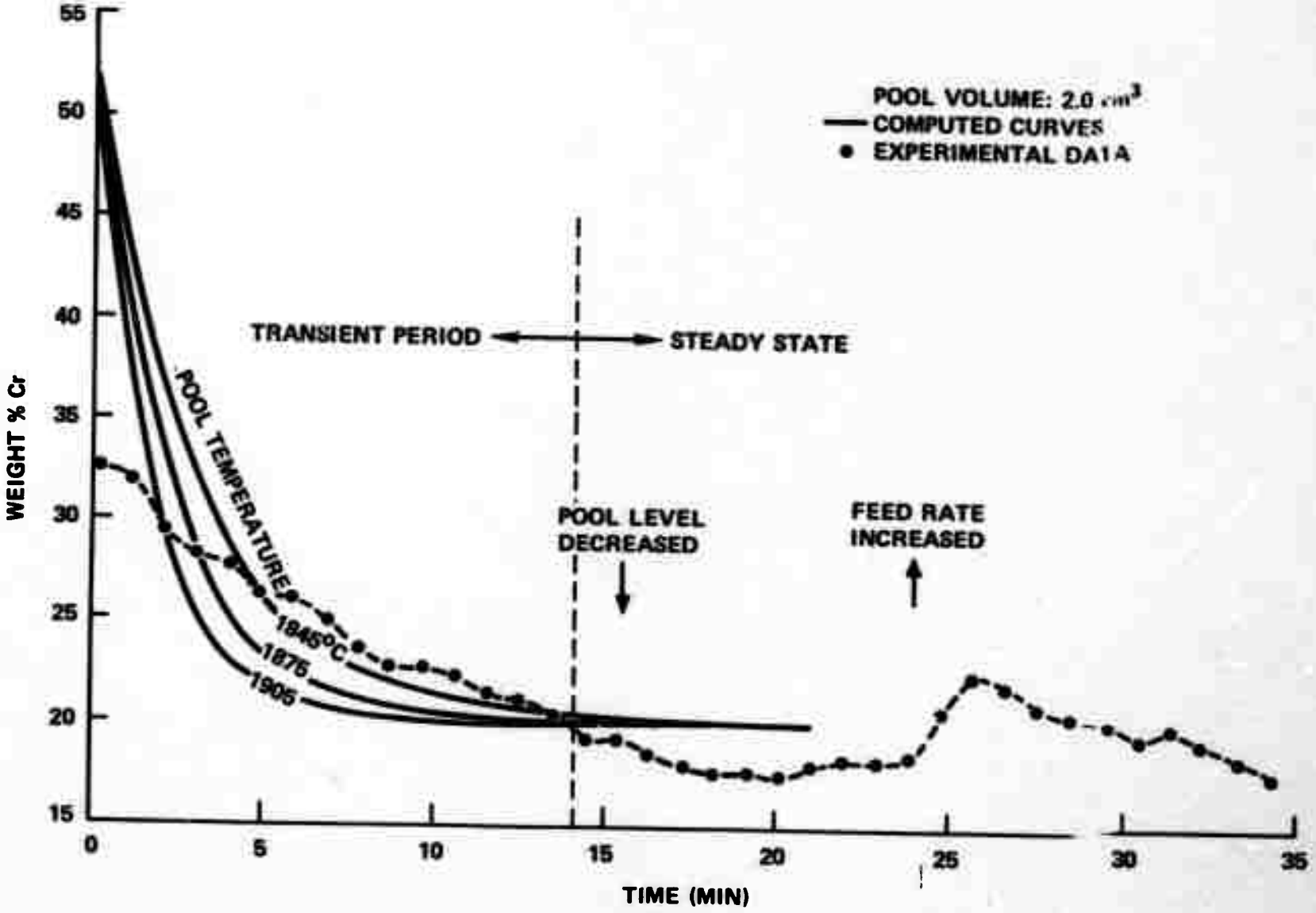

Figure 8. Change in Chromium Content of the Deposit with Time, for Different Pool Temperatures and Constant Pool Volume, 2.0 cm^3.

TABLE III

Effect of Evaporation Temperature and Volume of Liquid Pool on the Length of Transient Period

Volume of Liquid Pool (cm^3)	Temperature of Evaporation 1665°C			1800°C			1875°C		
	Computed Time to reach		Experimental Length of transient period (min)	Computed Time to reach		Experimental length of transient period (min)	Computed Time to reach		Experimental length of transient period (min)
	20% Cr (min)	21% Cr (min)		20% Cr (min)	21% Cr (min)		20% Cr (min)	21% Cr (min)	
0.5	36	21		7.5	4.5		4	2	
1.0	75	42		15	9		7.5	4.5	
1.5	112	63		22.5	13.5		12	6.5	
1.75	127	74	>60	28	16				
2.0	145	84		30	18	24	16.5	8.5	14
2.25	163	95		36	20.5				
2.5	181	105		40	22.5		20	11	
3.0	218	126		48	27		25	13	
3.5				56	31.5		28	15	
4.0	290	168		64	36		33	17	
5.0				80	45		41	21.5	

substantiates the proposed model. The effect of errors in temperature measurement on the length of computed transient period is shown in table IV. The errors are more significant at lower pool temperatures.

B. Composition of the deposit:

1. Transient Period

In the initial stages, (e.g. Fig. 6, 0 to 4 minutes), the % Cr in deposit is lower than the computed values. This is due to the fact that during this interval, the pool volume builds up from 0 to 2 cc. During the remainder of the transient period, (Fig. 6, 4 to 14 minutes) the pool composition follows the computed curve well within the precision of the data. From Fig. 8, a variation in pool temperature of $\pm$ 30°C corresponds to a $\pm$ 3% variation in % Cr. This is about the scatter between computed and experimental values in Fig. 6. Similarly Figures 4 and 7 show good agreement between computed and experimental results, for a lower pool temperature, 1665°C.

2. Steady-State Period

The computed feed-rate of the rod decreases during evaporation until steady state is reached and then remains constant. Thus at 1800°C, the feed rate changes from 2.3 cm/hr, at the start of evaporation to 1.6 cm/hr in the steady state. Therefore, it is difficult to manually control the feed rate since it changes and also because it is very low. As shown in Figures 5 and 6, these errors due to feed rate control, are magnified in the "steady state" because of the lower Cr content in the pool. Even small errors in the feed rate grossly change the % Cr in the pool and hence in the deposit. The points at which feed rate is changed are indicated in Figures 5 and 6. This demonstrates the need for a more sensitive method of adjustment of the feed rate. With careful control, even manually,

TABLE IV

Effect of Errors in Temperature Measurement on the Length of Transient Period

Volume of Liquid Pool (cm^3)	Temperature of Pool (°C)	Computed Time to Reach	
		20% Cr (min)	21% Cr (min)
1.75	1635	184	107
	1645	162	94
	1655	143	83
	1665	127	74
	1675	113	65
	1685	100	58
	1695	89	51
2.0	1845	21	11.5
	1855	19.5	10.5
	1865	18	9.5
	1875	16.5	8.5
	1885	15	7.75
	1895	13.5	7
	1905	12.5	6.5

± 1% Cr fluctuation in deposit can be maintained which is the amount allowed by ASTM Standard B-344-59I.

VI. SUMMARY AND CONCLUSIONS

A theoretical model has been developed for alloy evaporation from single rod-fed electron beam sources. The model permits us to calculate the composition of the molten pool and deposit at various times and the length of the transient period at various pool temperatures.

Experiments were carried out for the evaporation of a Ni-20Cr alloy at three different temperatures and the lengths of transient periods were determined. The experimental results agree closely with the theoretical estimates. This validates the thermodynamic data on activities of Ni and Cr in Ni-Cr alloys at 1600°C and the regular solution assumption used. The model may be used to predict evaporation behavior from a single source in any alloy system.

At higher evaporation temperatures, the times necessary for the pool to assume steady state composition are small, about 15 minutes for Ni-20Cr alloy. This makes the process economically attractive. The importance of accurate adjustment of feed rate is demonstrated.

REFERENCES

1. Smith, H.R., et al., Journal of Vac. Sci. Tech., 7, S48, 1970.

2. Santala, T., and Adams, C.H., Journal of Vac. Sci. Tech., 7, S22, 1970.

3. Langmuir, I., Phys. Rev. 2, 329, 1913.

4. Hirth, J.P., and Pound, G.M., "Condensation and Evaporation," MacMillan, New York, 1963, p. 80.

5. Holland, L., "Vacuum Deposition of Thin Films," Chapman and Hall Ltd., London, 1966, p. 104.

6. Honig, R.E., and Kramer, D.A., Techniques of Metals Research, Ed. R. Bunshah, Vol. IV, pt. 1, 1970, p. 505.

7. Darken, L.S., and Gurry, R.W., "Physical Chemistry of Metals," McGraw Hill Book Co. Inc., New York, 1953, pp. 266-270.

8. Gilby, S.W., and St. Pierre, G.R., Trans. Met. Soc. AIME, 245, 1969, PP. 1749-1763.

9. McElroy, D.L., and Fulkerson, W., Techniques of Metals Research, Ed. R. Bunshah, Vol. I, pt. 1, 1968, pp. 215-222.

10. Kennedy, Kurt, "Alloy Deposition from Single and Multiple Electron Beam Evaporation Sources," AVS Regional Symposia, 1968.

Part I

Supplement 2

The Effect of Substrate Temperature on the Structure of Titanium Carbide deposited by Activated Reactive Evaporation

I. INTRODUCTION

Structure controls many properties of the materials (e.g. physical, mechanical, electrical, magnetic, etc.). Study and control of the structure have been largely instrumental in the development of materials with desired properties. Similar studies on the structure of condensed materials have also been of great interest for the past two decades. Many authors have considered the initial growth and structure of evaporated films, and several useful review articles have been written on various aspects of the subject.[1,2] However, most of the existing studies are mainly concerned with thin films with the exception of a few on thick deposits.[3,4,5]

The present study was undertaken to study the effect of substrate temperature on the structure of titanium carbide deposited by Activated Reactive Evaporation (ARE) technique.

The deposits were characterized by microstructure, preferred orientation, lattice parameter and microhardness measurements.

II. EXPERIMENTAL TECHNIQUES

In the Activated Reactive Evaporation (ARE) process,[6] a reaction between metal vapor atoms and gas molecules results in the formation and deposition of a compound. To this extent, it is similar to the Reactive Evaporation process. The ARE process has been developed to produce a high deposition rate of a compound. Therefore, the metal vapor density

and the gas molecule density in the reaction zone must be sufficiently high to provide a high collision frequency between the reacting species. In our case, see Fig. 1, the high vapor density is provided by an electron beam heated pool of molten metal or alloy contained in a water-cooled copper crucible. The reactive gas is introduced at a high partial pressure ($\sim 10^{-4}$ torr) in the chamber. The reaction zone is located above the metal vapor source and below the substrate.

A high collision frequency does not insure a high reaction rate between the components. For many cases, e.g. $2Ti+C_2H_2 \rightarrow 2TiC+H_2$, the reaction has to be stimulated by activating one or both of the reactants. In the ARE process, this is done by placing an electrode at a + ve potential ($\sim$100 to 250 V) above the pool. This draws the primary and secondary electrons above the pool into the reaction zone thus ionizing and activating the reactants. For high rate deposition of a compound, it is essential that "activation" of the reactants occurs in the reaction zone. Variations of the Reactive Evaporation process proposed in the literature have activated the reacting gas by a glow discharge or microwave discharge outside the reaction zone.[7] This would not be sufficient for a high rate of deposition of the compound since activated gases become deactivated on collision with other gas molecules or surfaces in the gas path e.g. the tube through which the gas flows.

The evaporant was titanium (Grade Ti A40), in the form of a rod of 0.975" diameter. The chemical analysis of the titanium used is given in Table I.

The titanium carbide deposits were collected on a 2 mil thick tantalum foil 1" x 3", positioned 6" directly above the molten pool. The substrate was heated by direct resistance heating of the tantalum foil with a 4 kW

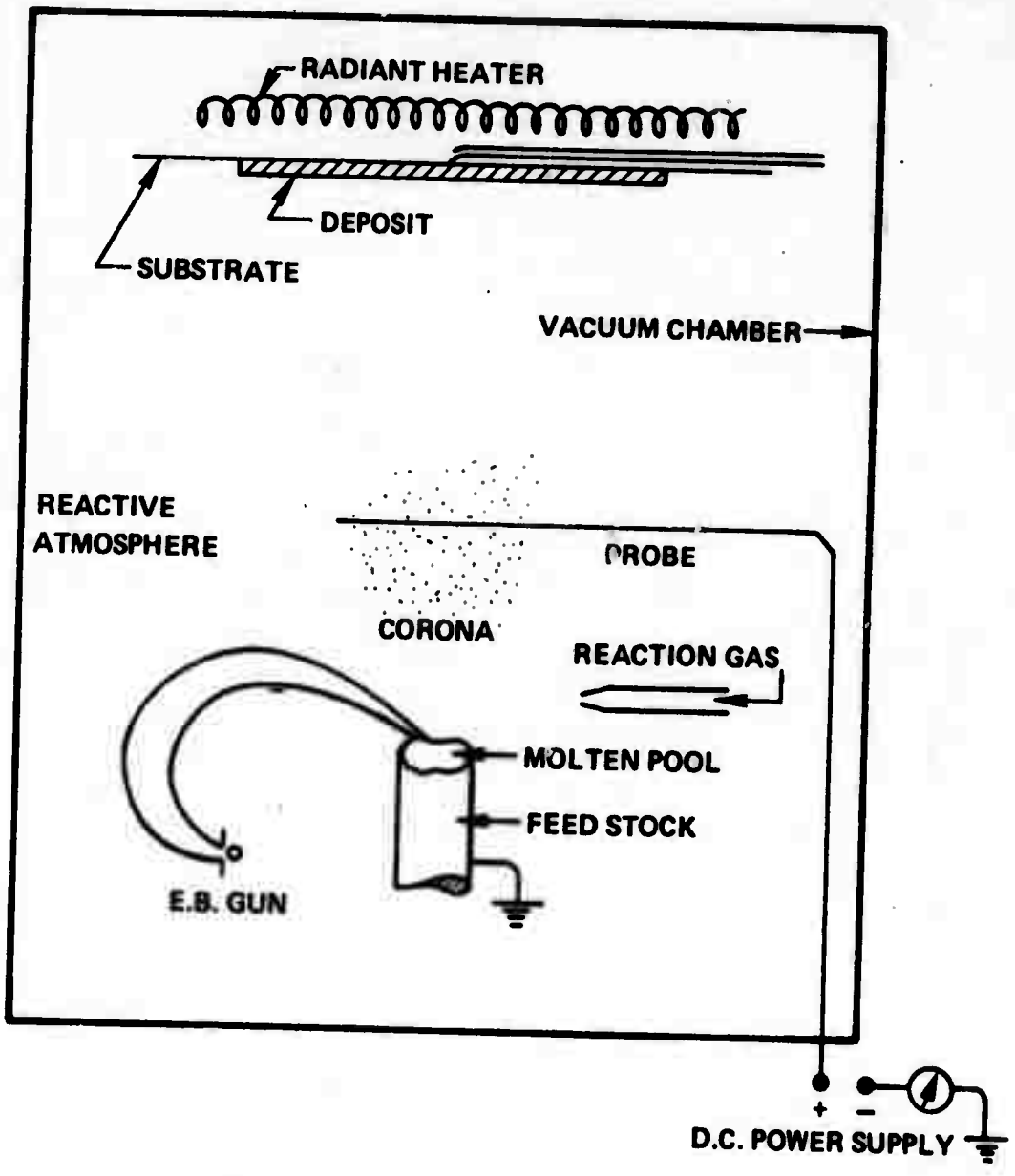

Figure 1. Activated Reactive Evaporation – Schematic

Table I

Chemical Composition of the Titanium Billet

Al	<.05
Fe	.043
Cu	<.01
Cr	<.025
Mn	<.05
Mo	<.025
Sn	<.1
V	<.05
C	.010
O	.118
N	.011
H	.0010
Ti	balance

power supply. The substrate temperature was measured with a Pt/Pt-10%Rh thermocouple placed in contact with the back side of the substrate. The deposition temperature was varied from 500°C to 1450°C.

In all evaporations the temperature of the pool was maintained constant at 1870°C with a constant evaporation rate of 0.66 g/min. The pressure of the reactive gas, C_2H_2, was also maintained constant at 4×10^{-4} torr as measured by a hot cathode ionization gauge.

The deposits were identified by x-ray diffraction analysis carried out on a Norelco x-ray diffraction unit using CuK_α radiation with a nickel filter. For accurate determination of the lattice parameter, the unit was aligned using a standard tungsten specimen. The lattice parameter was determined using only high angle peaks (i.e. $2\theta > 90°$) and $\cos\theta \cot\theta$ extrapolation technique. The precision of the data is within $\pm$ 0.0002Å.

Microhardness measurements on the deposits were carried out on a Kentron microhardness tester, using both diamond pyramid and Knoop indentors at loads of 50 & 100g. The diagonal lengths of the indentations varied from 4 μm to 6 μm for pyramid indentations and 11 μm to 23 μm for Knoop indentations. The maximum depth of indentation was calculated to be less than 1.5 μm. In each case a number of measurements were made. Since TiC is very hard and brittle, there was considerable scatter in the results, the maximum scatter being about $\pm$ 10% of the mean value.

III. RESULTS AND DISCUSSION

A. Rate of Deposition vs. Substrate Temperature:

The rate of deposition decreased with increasing substrate temperature, for a constant rate of evaporation of titanium. The results are tabulated in Table II and plotted in Fig. 2. In the temperature range of 520°C to 1450°C, the rate of deposition decreased linearly with increasing temperature. Langmuir[8] considers this as a phenomenon of condensation and

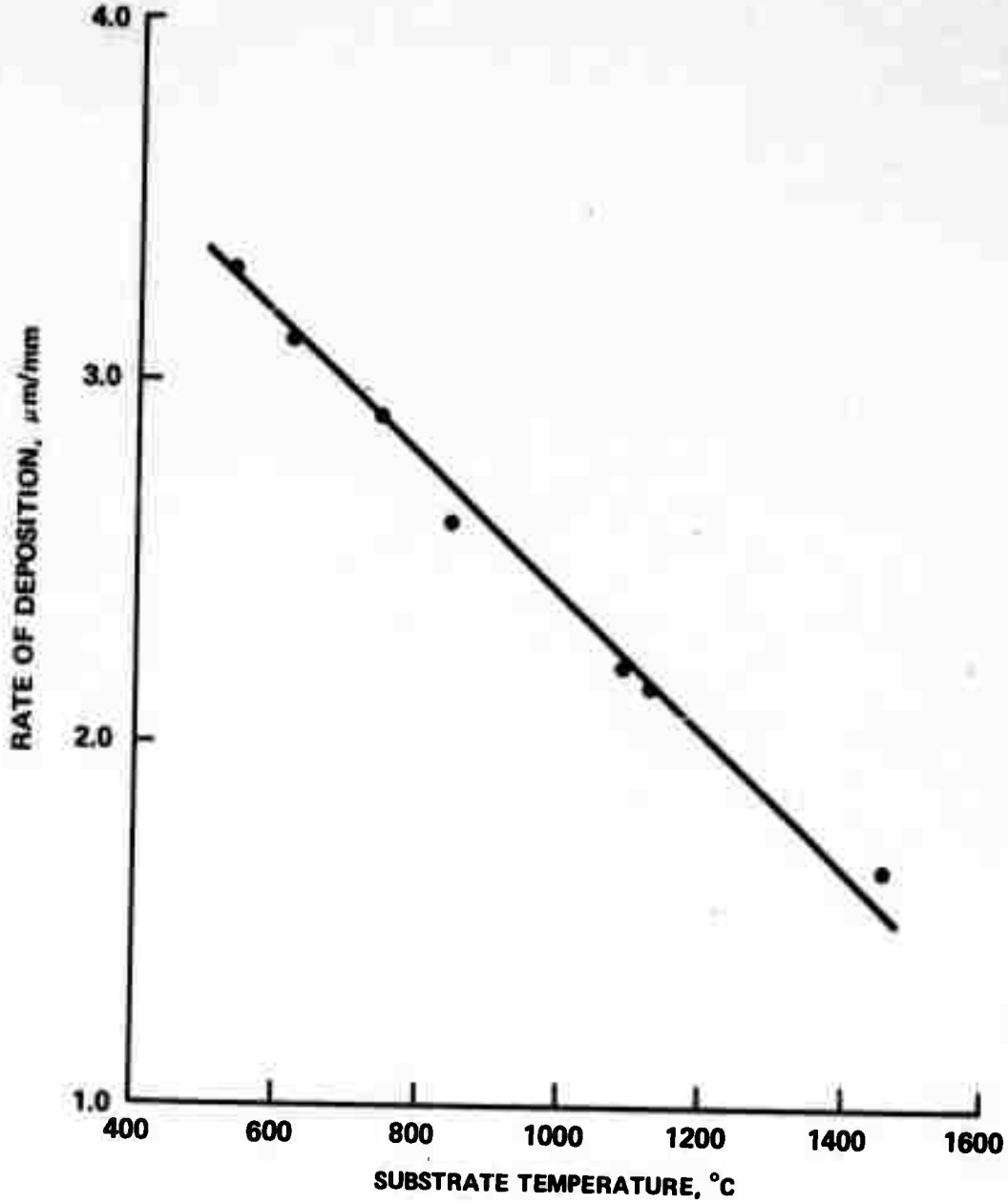

Figure 2. Rate of Deposition vs. Substrate Temperature for TiC

Table II

Rate of Deposition of TiC at Different Substrate Temperatures

Substrate Temperature °C	Thickness of Deposit µm	Duration of Deposition min	Rate of Deposition µm/min
520	100.0	30	3.3
610	93.0	30	3.1
730	87.5	30	2.9
830	67.5	26	2.6
1080	37.5	17	2.2
1120	30.0	14	2.15
1450	55.0	30	1.85

re-evaporation. According to this theory a vapor atom has an average life on a surface on which it impinges before it re-evaporates. The average life of the vapor atom will be longer and condensation will be more likely, the more intense the forces binding the atom to the substrate and the lower the substrate temperature. Thus, at constant evaporation rate for the same substrate material, the average life on the surface is shorter at the higher temperature which in turn increases the probability of re-evaporation, giving rise to lower deposition rates at higher temperatures.

B. Preferred Orientation vs. Substrate Temperature:

Vapor deposited films are well known to have varying amounts of preferred orientations in them. Thus, a qualitative study of preferred orientation in the titanium carbide deposits were made by considering the relative x-ray intensities perpendicular to the surface for the first ten reflections. The results are shown in Fig. 3 along with the intensities for a random polycrystalline sample.[9] It can be seen from this figure, that considerable amounts of preferred orientation in {220} plane exists at temperatures below 830°C. As the temperature is increased, the texture transforms to a random texture. This is similar to the trend observed by Kennedy[5] on iron and iron-10% nickel deposits.

C. Lattice Parameter vs. Substrate Temperature:

The lattice parameters of the deposits at various substrate temperatures are tabulated in Table III, and shown in Fig. 4. Fig. 4 is a plot of lattice parameter versus the carbon to metal ratio, [C/M] from the published data[10,11], which shows considerable scatter at high [C/M] ratios. Our data are shown as two bands on Fig. 4. Estimating the [C/M] ratios from the published data in Fig. 4, the low temperature deposits (i.e. at

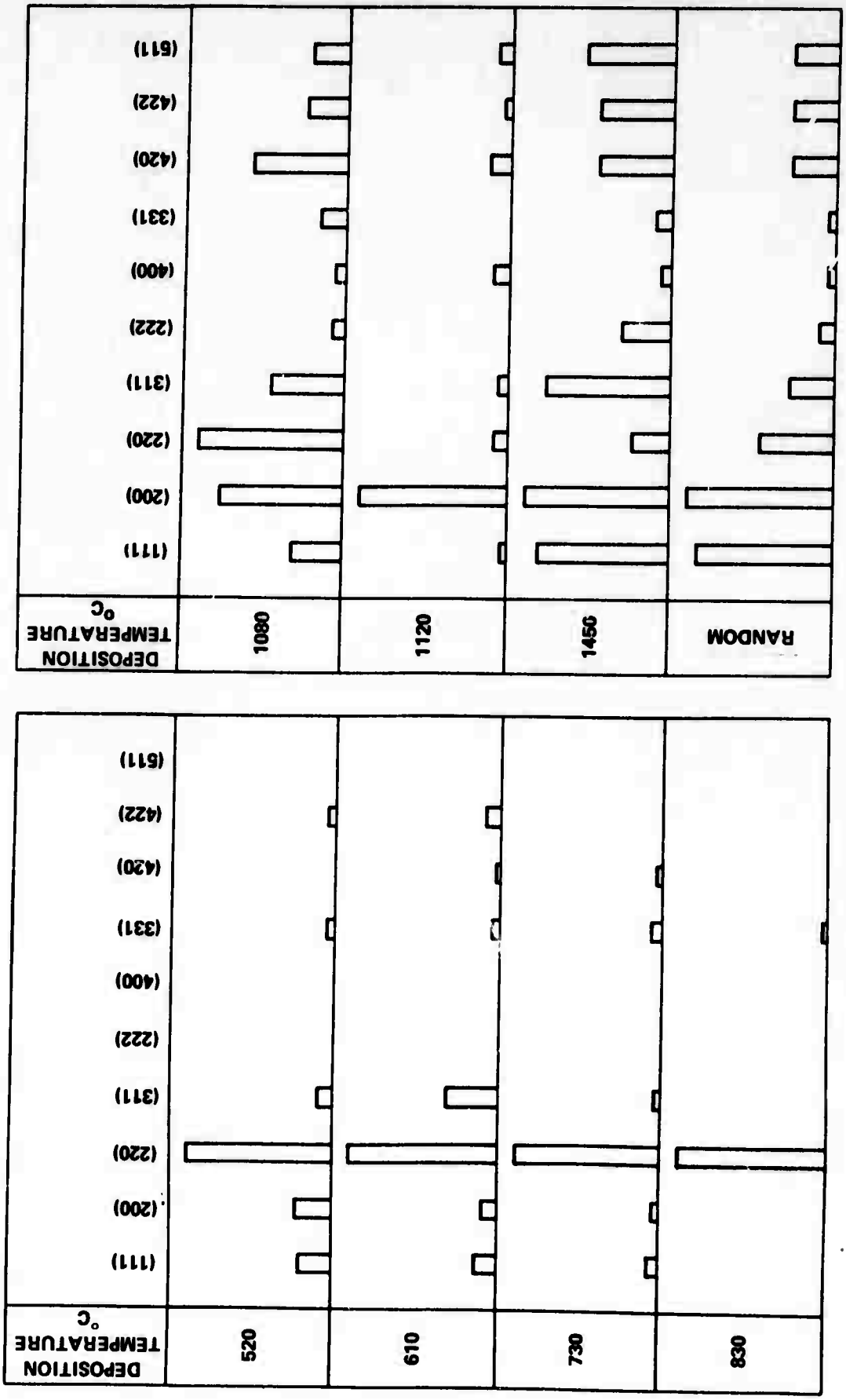

Figure 3. Relative Intensities of X-Ray Diffraction Peaks from TiC Deposits at Different Substrate Temperatures

Table III

Lattice Parameter and Microhardness of TiC Deposits at Different Temperatures

Deposition Temperature °C	Thickness of Deposit μm	Lattice Parameter Å	Microhardness 50 g load DPHN	KHN	100g load KHN
520	100	4.3250	2710	2630	2900*
610	93	4.3245	2330	2580	2870*
730	87.5	4.3282	2955	3720	2940
830	67.5	4.4293	2955	3480	3141
1080	37.5	4.3290	4110	5520	4036
1120	30.0	4.3280	4160	5430	3840
1450	55.0	4.3287	3890	4900	4270
500°C-annealed at 1180°C 1 hr.	100.0		3565	5440	5118
520 (ref.6)	100.0	4.3283	2900		
Ta substrate			100		150

*large cracks observed at the ends of the diagonal.

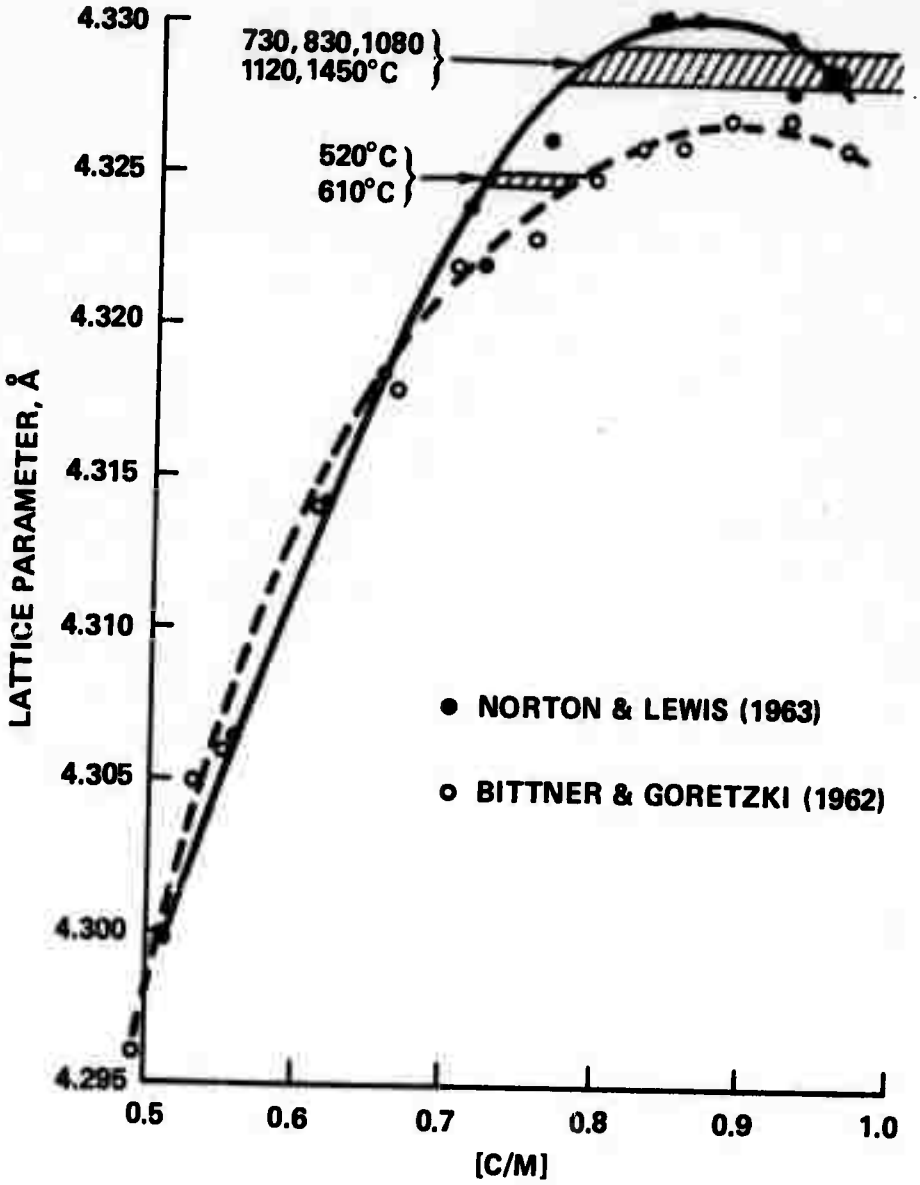

Figure 4. Lattice Parameter vs. [C/M] Ratio for TiC

520 and 610°C) show lattice parameters corresponding to C/M ratio of 0.72 to 0.77 and the high temperature data (i.e. 730, 830, 1080, 1120 and 1450°C) show lattice parameters corresponding to C/M ratios of 0.8 - 0.95. It was intended to keep the lattice parameter constant for all deposition temperatures. Due to some unexplained variation in the present set of experiments, the lattice parameters of the deposits at the two lowest temperatures are somewhat lower than the others, see Table III. TiC deposits with lattice parameters around 4.3280Å and DPH of 2900 kg/mm^2 have been produced even at 520°C in the past under similar conditions.[6] Since lattice parameters are sensitive to the carbon content and impurity content (e.g. O_2 and N_2) of TiC, a precise correlation between lattice parameter, [C/M] ratio and impurity content depend on obtaining reliable analytical data and will be the subject of a future investigation. Norton and Lewis[9] show a maximum value of a_o = 4.3305Å at $TiC_{0.88}$ decreasing to a_o = 4.3280Å at $TiC_{1.0}$. Our values, Table III, are much closer to the latter.

D. Structure of the Deposits vs. Substrate Temperature:

Fig. 5a and 5b shows a series of optical and scanning electron micrographs of titanium carbide deposits at different substrate temperatures. These micrographs show the structure of the deposited surface and across the fractured thickness of the deposit. At low temperatures, say T_b < 520°C, the surface has a characteristic domed structure. The cross-section of the low temperature deposits consists of very fine tapered grains, the width of the grains increasing in the growth direction. As the substrate temperature is increased above T_b > 610°C, the domed structure disappears. The high temperature deposits show columnar grains across the cross section which are equiaxed when viewed on the deposit surface. A further increase in substrate temperature coarsens the columnar structure, the width of the columns increasing with increase in substrate temperature.

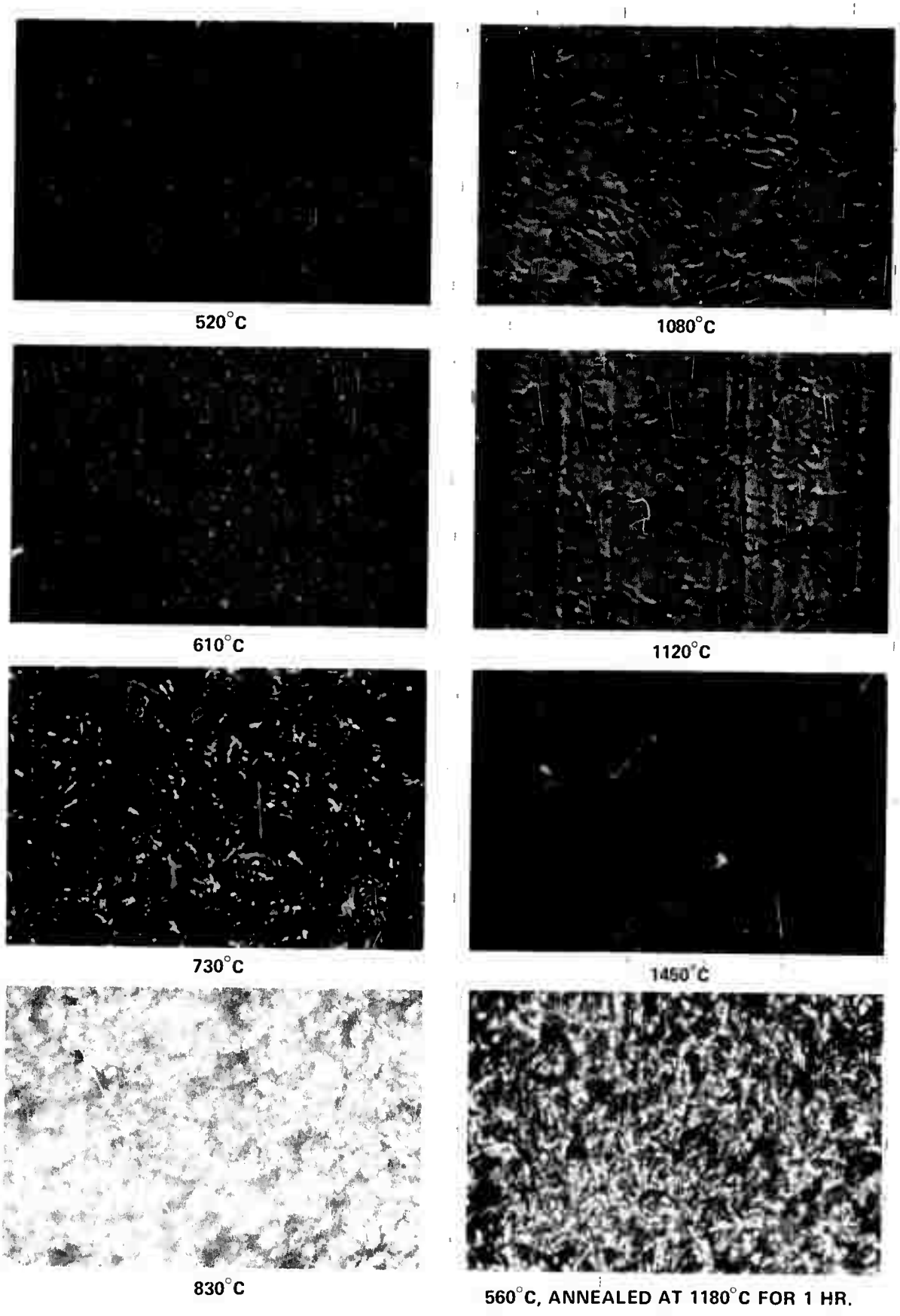

Figure 5(a). Optical Micrographs of TiC Deposits at Different Substrate Temperatures. Unetched Deposit Surface. Magnification 1100

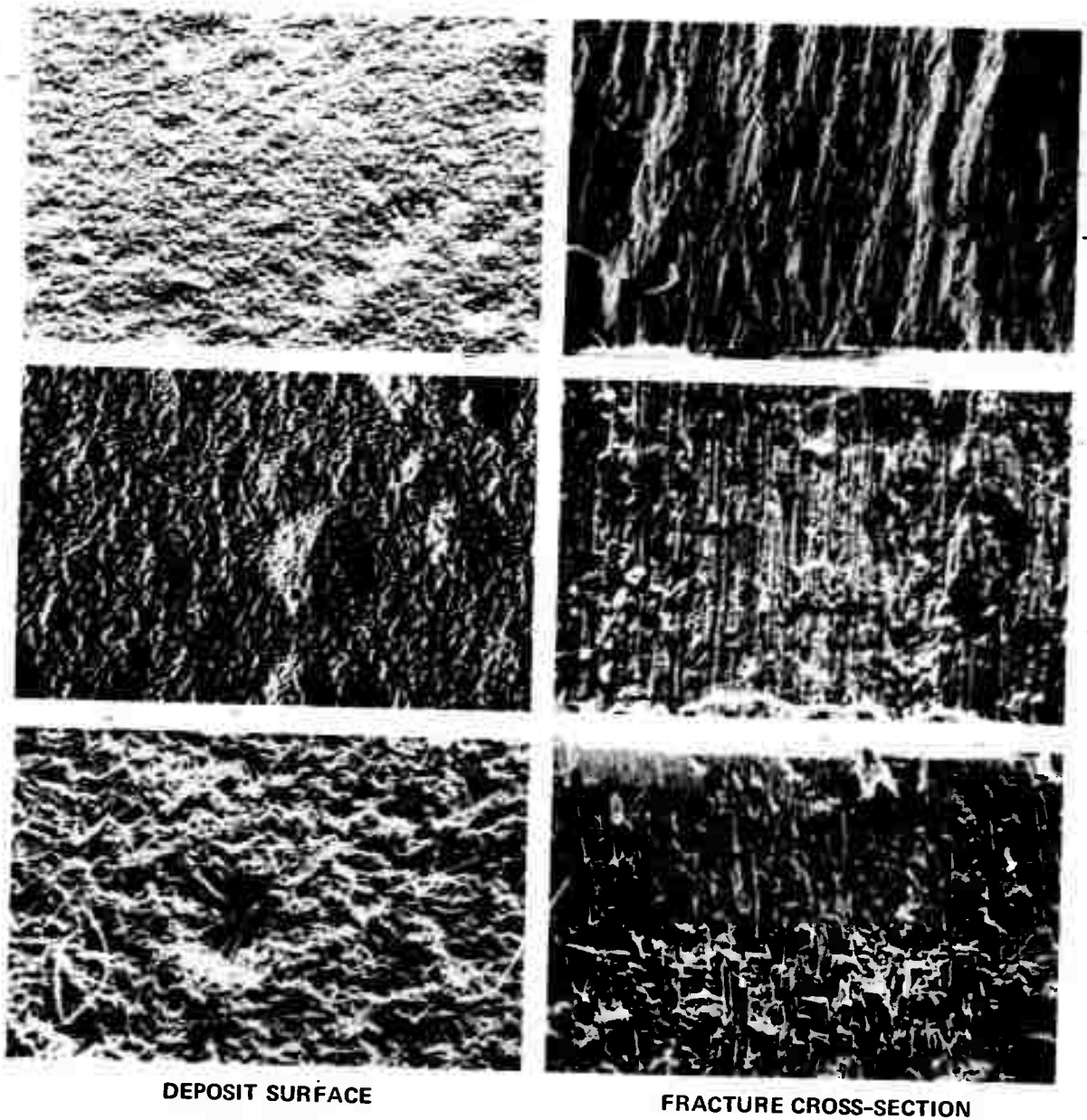

DEPOSIT SURFACE

FRACTURE CROSS-SECTION

DEPOSITION TEMPERATURE °C	LATTICE PARAMETER °A	MICROHARDNES 50 g LOAD	
		DPHN	KHN
520	4.3250	2710	2630
610	4.3245	2330	2580
730	4.3282	2955	3720

Figure 5b: Scanning Electron Micrographs of TiC Deposits at Different Substrate Temperatures, X 1000.

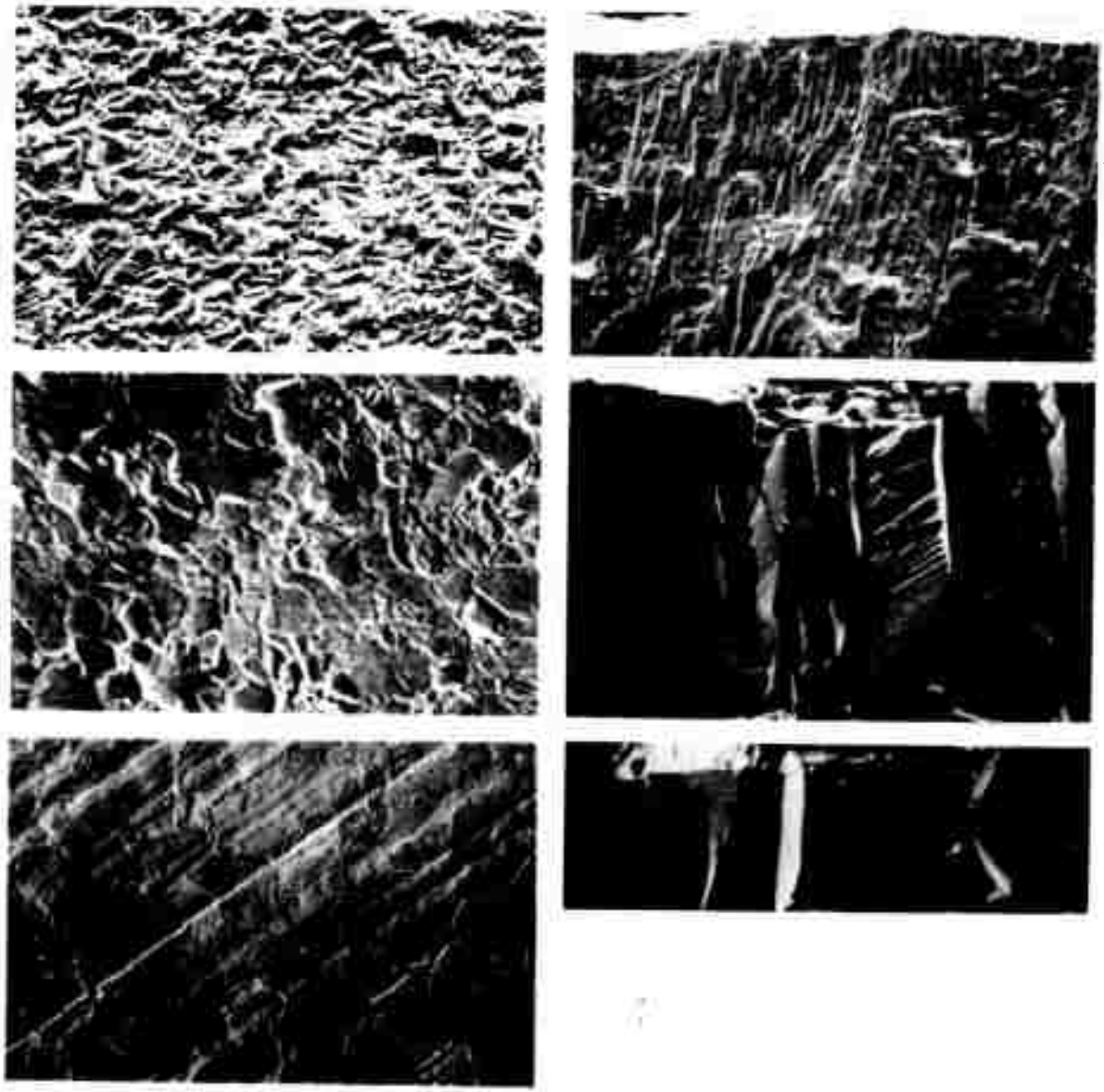

DEPOSITION TEMPERATURE °C	LATTICE PARAMETER A	MICROHARDNESS 50 g LOAD DPHN	KHN
830	4.4293	2955	3480
1080	4.3296	4110	5520
1120	4.3280	4160	5430

DEPOSIT SURFACE

FRACTURE CROSS-SECTION

Figure 5b: Scanning Electron Micrographs of TiC Deposits at Different Substrate Temperatures, X 1000.

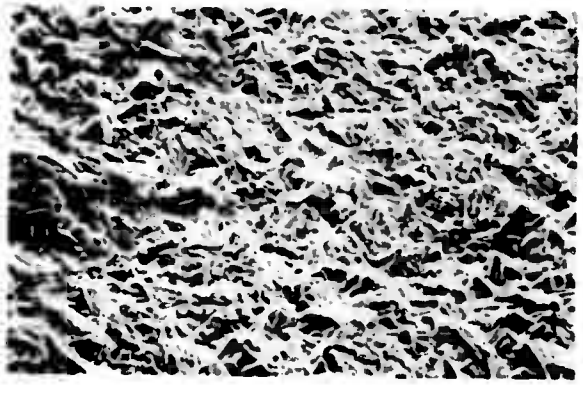

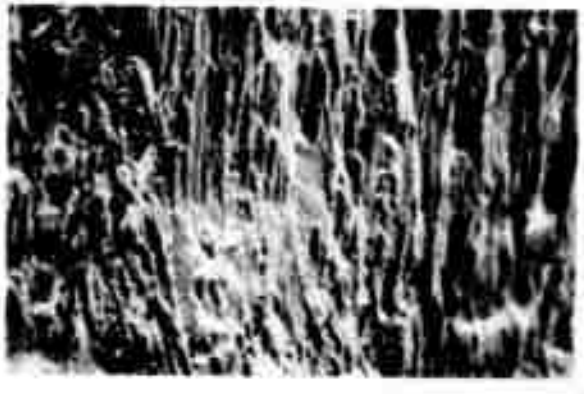

DEPOSIT SURFACE

FRACTURE CROSS-SECTION

DEPOSITION TEMPERATURE °C	LATTICE PARAMETER Å	MICROHARDNESS 50 g LOAD DPHN	KHN
1450	4.3287	3890	4900
DEPOSIT AT 560° ANNEALED AT 1180° C	—	3585	5440

Figure 5b. Scanning Electron Micrographs of TiC Deposits at Different Substrate Temperatures, X 1000

Bunshah and Juntz[3] studied the influence of condensation temperature on microstructure of titanium sheets. They reported the change in surface morphology of the deposited sheets with temperature. They observed columnar structure with increasing grain size with increase in substrate temperatures from 450°C up to 750°C, around 840°C a predominent whisker growth at the vapor-solid interface with subsequent thickening, from 883 to 880°C a coarse columnar Alpha and above 883°C a "transformed Beta" structure. The change in morphology was gradual from one type to the next.

Movchan and Demchishin[4] have studied titanium, nickel, tungsten, alumina and zirconia deposits on a substrate with a temperature gradient and established three characteristic structural zones, schematically shown in Fig. 6. Zone 1 consists of domed structure, zone 2 shows columnar grains with a smooth surface and zone 3 is a characteristic polyhedral structure. The temperature ranges reported by them are:

	Zone 1	Zone 2	Zone 3
Metals	$<0.3\ T_m$	$0.3\text{-}0.45\ T_m$	$>0.45\ T_m$
Oxides	$<0.26\ T_m$	$0.26\text{-}0.45\ T_m$	$>0.45\ T_m$

T_m is the melting point of the material in °K. They attribute the changes in surface morphology to different condensation mechanisms, i.e. vapor-liquid-solid or vapor-solid and the absence of surface diffusion at low temperatures.

Similar observations were made by Kennedy[5] on Fe, Fe-10%N and Fe-1%Y deposits. He observed columnar grain structure and large preferred orientations at low substrate temperatures and more randomly oriented structure at high substrate temperatures.

Our study on titanium carbide is also in the same direction as the results discussed above, however, in the substrate temperature range reported here 520° - 1450°C or .25-.52 T_m, we have observed only the first two zones of the three reported by Movchan and Demchishim.[4]

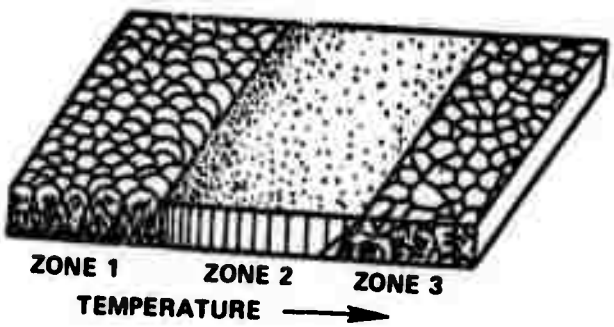

Figure 6. Schematic of Structural Zones of Condesates at Different Substrate Temperatures

It is very probable that the number of zones, type of structures, their orientation and grain size are very intimately related to the purity of the deposit purity and the surface condition of the substrate, the bonding between the deposited material and the substrate material, residual stresses, possible solid-solid transformations in the deposit and the rate of deposition. Further experimentation is needed to sort out the important variables controlling structure.

E. Microhardness vs. Substrate Temperature:

The results of the microhardness measurements on titanium carbide are tabulated in Table III and shown in Fig. 7 as a function of substrate temperature. The 50g and 100g loads gave very similar microhardness values. Both diamond pyramid and the Knoop hardness values increase with increase in substrate temperature. The results show a phenomenal increase in the microhardness with increase in substrate temperature similar to the results reported for alumina and zirconia.[4] Maximum diamond pyramid hardness is 4160 kg/mm^2 and maximum Knoop hardness is 5520 kg/mm^2. In earlier work, Williams and Lye[12] showed also that hardness measured with the Knoop indenter is higher than the values obtained with the diamond pyramid indenter on the same TiC sample. Even with the large scatter, these results are much higher than the earlier reported maximum microhardness of 3200 kg/mm^2 at 50g load for titanium carbide.[13] The tantalum substrate has a diamond pyramid hardness of 100 kg/mm^2 and a Knoop hardness of 150 KHN.

The value of lattice parameter and microhardness for deposit temperatures of 520 and 610°C are both lower than expected due to some unexplained variation in this experimental series as shown in Table III, indicating a lower [C/M] ratio. In previous work,[6] we obtained TiC deposits

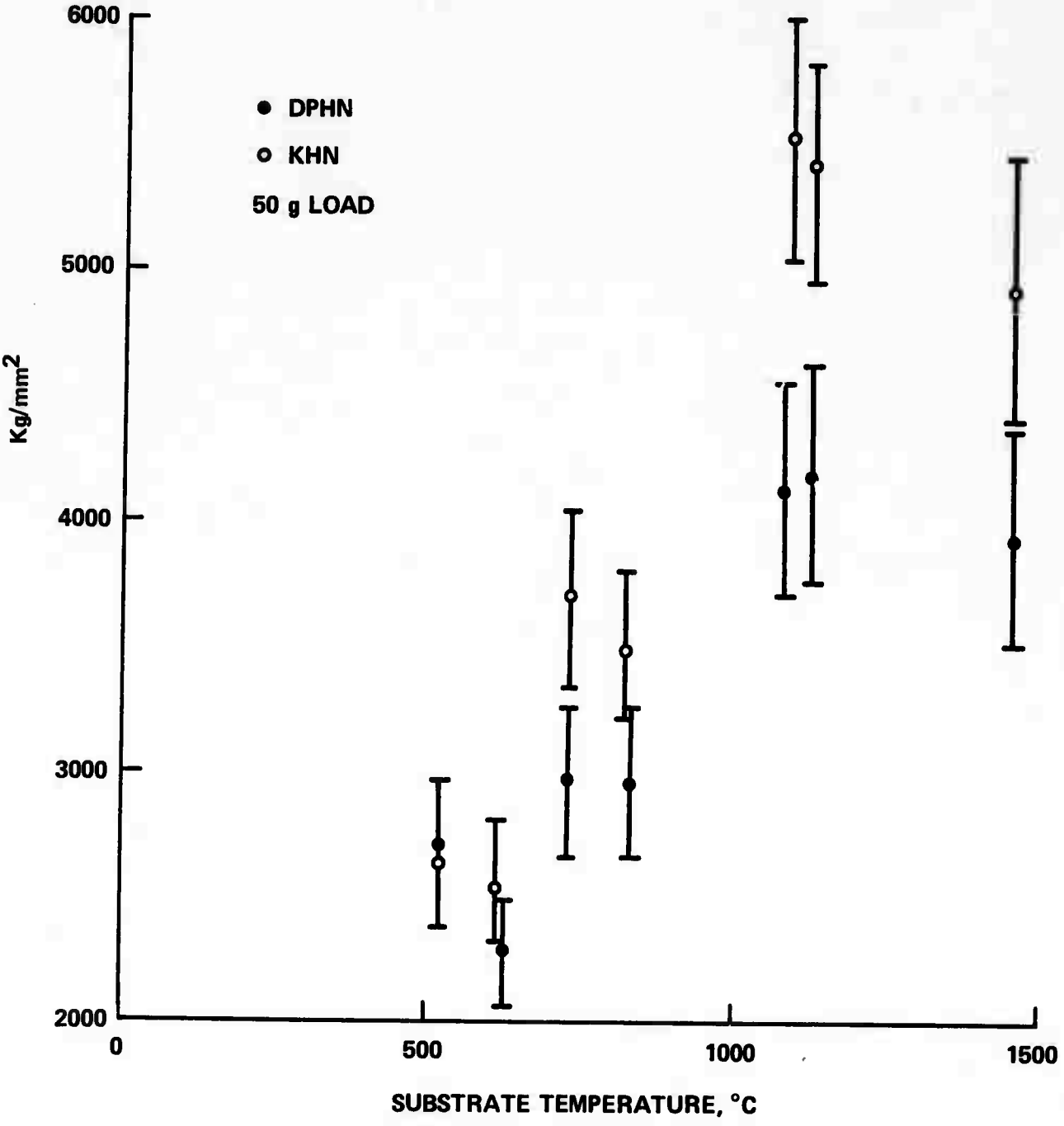

Figure 7. Microhardness of TiC Deposits at Different Substrate Temperatures

with lattice parameter of 4.3283Å and microhardness of 2775 kg/mm^2 at a deposition temperature of 520°C. This is in agreement with the observation that the microhardness increases with lattice parameter and [C/M] ratio.

It is interesting to note that the specimen deposited at 500°C and annealed in situ at 1180°C for 1 hour in the deposition chamber shows a high hardness and a structure corresponding to a high temperature deposit.

The following factors might have contributed to the enhanced microhardness reported in the present study for titanium carbide deposited directly on the substrate through a direct reaction between titanium atoms and carbon in C_2H_2 as compared to hot pressed or arc melted product:

1. Higher density and smaller defect concentration of the high temperature deposit as compared to powder compacted or arc cast material.
2. A different impurity content (e.g. O_2, N_2 or Ta) in the deposited material.
3. Residual stresses because of the mismatch in thermal coefficients of expansion between the TiC deposit and the Ta substrate. In this case, the mismatch about 15%.
4. Possible radiation damage by bombardment of the deposit from the ions in the reaction zone.
5. A different defect structure of the deposit.
6. Precipitation of carbon or other impurity associated phases.

IV. SUMMARY AND CONCLUSIONS

Titanium carbide was deposited on resistance heated tantalum substrates in the temperature range 520°C to 1450°C, by activated reactive evaporation.

It has been shown that the rate of deposition decreases linearly with increase in temperature of the substrate.

The deposits were highly textured and had a {220} preferred orientation up to about 830°C; further increase in substrate temperature showed random orientations of titanium carbide in the deposits.

Scanning electron micrographs show a domed structure of 520°C and further increase in temperature tend to produce well defined columnar grain structures. The columnar grain size increased with increase in substrate temperature.

Microhardness of the TiC deposits increased with increase in the substrate temperature. The maximum hardness of the deposits (DPHN = 4160 kg/mm^2 and KHN = 5520 kg/mm^2 at 50g load) was much higher than the earlier reported values (3200 kg/mm^2).

PART II

THE PROPERTIES OF RARE EARTH METALS AND ALLOYS
TASK IV

D. L. Douglass

REFERENCES

1. K.H. Greeland, Brit. J. Sci. Inst., 38, 1 (1961).

2. G.A. Bassett, J.W. Menter, and D.W. Pashley, Proc. Conf. on Structure and Properties of Thin Films, 11 (1959), J Wiley & Sons.

3. R.F. Bunshah and R.S. Juntz, to be published.

4. B.A. Movchan and A.V. Demchishin, Fiz. Metal. Metalloved., 28, No. 4, 653 (1969).

5. K. Kennedy, Trans. Intr. Vac. Met. Conf., American Vacuum Society, 195 (1968).

6. R.F. Bunshah and A.C. Raghuram, to be published.

7. B.B. Kosicki and D. Khang, J. Vac. Sci. Tech. 6, 592 (1969).

8. I. Langmuir, Proc. Nat. Acad. Sci., Wash., 3, 141 (1917).

9. ASTM Powder Diffraction File, Card No. 6-0614.

10. J.T. Norton and R.K. Lewis, NASA-CR-321, National Aeronautics and Space Administration, Washington D.C. (1963).

11. H. Bittner and H. Goretzki, Monatsh Chem., 93, 1000 (1962).

12. W.S. Williams and R.G. Lye, AFML-TDR-64-25, Part II, March 1965.

13. J.J. Gillman and B.W. Roberts, J. Applied Physics, 32, 1405 (1961).

PART II

THE PROPERTIES OF RARE EARTH METALS AND ALLOYS

TASK IV

D. L. Douglass

I. INTRODUCTION

Alloys of the γ'-type contain sufficient aluminum to permit a continuous film of Al_2O_3 to form during oxidation in air at high temperatures. The film is very protective at the temperature of oxidation due to the very low rates of ion migration through the film. However, upon cooling from the isothermal oxidation treatment, the film is subjected to large strains due to differences in the coefficients of thermal expansion between metal and oxide and the fact that the film is adherent to the substrate. These strains cause stresses that exceed the fracture stress, and thus the films spall from the metal quite readily.

The addition of minor amounts of rare earths and/or yttrium impart a remarkable resistance to film spalling for reasons unknown. It is the objective of this task to evaluate the oxidation behavior of Ni_3Al containing 0.5% Y or Gd and to determine the mechanism of the enhanced resistance to spalling of films formed on these alloys.

II. EXPERIMENTAL PROCEDURES

Prior attempts to hot-roll strip from arc-melted buttons of Ni_3Al-type alloys were unsuccessful. It was therefore decided that thin slabs of the alloys would be cut from the buttons and oxidized in the "as-cast" structure. The slabs were mechanically abraded on successively finer papers through 600 grit, polished on a wheel with 0.5 micron alumina, annealed 20 minutes at 900°C, and oxidized in a Harrop TGA.

TABLE I

X-Ray Diffraction Analyses of Oxides Formed on Ni_3Al-Type Alloys at 1200°C

Alloy	Oxidation History	Oxide Analyzed	Relative Intensity of Various Phases			
			NiO	Al_2O_3	$NiAl_2O_4$	Substrate
Ni_3Al	Preoxidized 1 hour then isothermally oxidized	spalled oxide	very strong	weak	medium	none
		in situ oxide	medium	weak	weak	very strong
Ni_3Al	No preoxidation; oxidized isothermally	spalled oxide	none	medium	strong	none
		in situ oxide	none	weak	none	very strong
Ni_3Al-0.5Y	No preoxidation	in situ oxide (no spalling)	strong	medium	strong	weak
Ni_3Al-0.5Y	No preoxidation	in situ oxide (no spalling)	medium	medium	strong	very strong

III. RESULTS

The transient oxidation behavior of nickel-base alloys during extended heatup usually results in copious formation of NiO prior to the formation of the alloying constituent oxide such as Cr_2O_3 or Al_2O_3. The previous work on Ni-20Cr alloys containing rare earths utilized a preoxidation treatment for 1 hour in which the samples were immersed directly into a furnace at the desired temperature.[1] The samples were then introduced into the Harrop unit, and after the approximate 30 minute heatup time, the isothermal tests were run at the desired temperature with the first weight gain measurements taken as those for one hour. This technique alleviated the problem of forming different oxides during the slow heatup. In other words, only those oxides formed at a given temperature presumably formed.

A similar procedure was used on the Ni_3Al alloys, but this method was abandoned due to an excessive amount of spalling upon cooling after the preoxidation treatment. Subsequent oxidation in the Harrop TGA resulted in a markedly different behavior than for those samples oxidized only in the Harrop Unit. A summary of X-ray diffraction data for the reference alloys, Ni_3Al, and the alloy containing 0.5% Y is given in Table I.

The Ni_3Al sample that was preoxidized prior to isothermal oxidation gained weight very rapidly initially during isothermal oxidation. The x-ray results show a large amount of NiO and very little Al_2O_3. This behavior is probably associated with the formation of a thin layer of Al_2O_3 and spinel during preoxidation, spalling of this layer, and subsequent oxidation of a nickel-rich substrate layer at the surface. In other words, the aluminum content of the alloy was lowered at the surface by spalling of the scale. Subsequent formation of Al_2O_3 then required

more time because aluminum had to diffuse from within the alloy to the surface where it could be oxidized. No NiO was detected in the sample of this alloy that was not preoxidized. The kinetics of oxidation were very low, but unfortunately, the protective scale spalled during cooling.

The presence of 0.5% Y resulted in very little spalling of the scale other than at some of the edges. A very small fraction, about 5% or less, of the scale spalled on the &-containing alloys.

Kinetics data were obtained on the four samples listed in Table I but will not be presented because there appeared to be an inclusion of unmelted nickel in the center of the button which negates the validity of the results. The inclusion had a thick black oxide, most likely NiO, and thus it will be necessary to remelt and retest this alloy. The kinetics data include a weight gain for a nickel-rich zone plus a weight gain for the remainder of the alloy, Ni_3Al.

REFERENCE

1. Bunshah, R.F., and Douglass, D.L., Technical Report UCLA-Eng-7161 September 1971.

PERSONNEL

The following personnel have been working on Part II of this program:

Principal Investigator: Professor D. L. Douglass

Graduate Student: Mr. J. R. Kuenzly